Network analysis of mesoscale mouse brain structural connectome reveals modular structure that aligns with anatomical regions and sensory pathways

Short Title: **Network analysis of mesoscale mouse brain connectome.**

Bernard A. Pailthorpe
Brain Dynamics Group,
School of Physics.
University of Sydney.
NSW. 2006. Australia.
email: bernard.pailthorpe@sydney.edu.au

Abstract
The Allen mesoscale mouse brain structural connectome is analysed using standard network methods combined with 3D visualizations. The full region-to-region connectivity data is used, with a focus on the strongest (top 40%) structural links. The spatial embedding of links and time evolution of signalling is incorporated, with two-step links included. Modular decomposition using the Infomap method produces 8 network modules that correspond approximately to major brain anatomical regions and system functions. These modules align with the anterior and posterior primary sensory systems and association areas. 3D visualization of network links is facilitated by using a set of simplified schematic coordinates that reduces visual complexity. Selection of key nodes and links, with a focus on primary sensory pathways and cortical association areas, together reveal structural features of the mouse structural connectome consistent with biological functions in the sensory-motor systems, and selective roles of the anterior and posterior cortical association areas of the mouse brain. The fabric of weaker links generally are longer range with some having brain-wide reach. Cortical gradients are evident along sensory pathways within the structural network.

Author's Summary
Network models incorporating spatial embedding and signalling delays are used to investigate the mouse structural connectome. Here computational method work like experimental probes to uncover biologically relevant features. I use the Infomap method, which follows random walks on the network, to decompose the directed, weighted network into 8 modules that align with classical brain anatomical regions and system functions. Primary sensory pathways and cortical association areas are separated into individual modules. Strong, short range links form the sensory-motor paths while weaker links spread brain-wide, possibly coordinating many regions.

Introduction
Major projects to map brain structure in a variety of animals are producing significant datasets laying out structural and functional connectivity [1] patterns that present challenges for analysis [2, 3]. Methods from network science [4, 5] can shed light on important hubs, links and modular sub-divisions. These can be characterised using tools derived from the mathematical apparatus of graph theory [2-6]. Ultimately functional circuits may be resolved, as are being painstakingly reconstructed using

modern experimental probes (e.g. see [8]). The challenge is to find appropriate network models that can realistically reproduced/predict brain structural and functional connectivity data.

Here the Allen Institute for Brain Science (AIBS) dataset of a mesoscale structural connectome for the mouse brain [9] is studied using a combination of data analytical, network and visualization methods. While the data is brain wide it is at the meoscale (resolution of 0.1 mm voxels and 0.35 mm coronal plane imaging), in which links involving many neurons are probed. Connectivity data at finer scales, at the level of individual neurons and synapses, are available for smaller samples, such as with mouse retina [10, 11]. Higher resolution data also is emerging at the level of cortical layers [14]. These studies shed light on the correlation between structural and functional connections between nodes in the mouse brain. The nodes are located at known 3D coordinates from the Allen Atlas [13]. Typically the sources and targets of the probed connections are classical anatomical regions that, given sampling protocols, vary significantly in size and functional significance. That non-uniform sampling presents challenges for analysis [15]. Already some network methods have been applied to the AIBS mouse connectome to find the basic network features [9, 16] or to infer hubs via their transcriptional signatures [17], especially in the cortex – these studies show consistency with a Watts-Strogatz small world and rich club connectivity. Sampling statistics, thresholding and possible roles of weak links have been studied [18].

This study: revisits the definition of link weights; explores what types of network models are best suited to analyse the single hemisphere mouse connectome; uses random walk based information-theoretic methods to perform modular decomposition; develops computational probes of sensory – motor – association pathways, inspired by traditional experimental probes, to explore signalling pathways; and explores correlations with other cortex/brain gradients.

It is becoming increasingly evident that brain connectivity comprises more than a simple network. The links are directed and weighted, they can be signed: that is excitatory or inhibitory, they also can be modulated by chemicals (neuromodulators, hormones, etc) present in the extracellular space, the links have spatial extent and fit within a finite volume, and the links can be activated over time. There may be several types of networks present that operate separately or in parallel [19]: the emerging theory of multi-layer networks [20, 21] provides tools for such analysis as relevant data becomes available. Continuing developments in network theory show the need for network models to be tailored to suit the processes occurring in the system under study (i.e. transport, social interactions, information transmission, etc.). While for transport networks the underlying transmission mechanisms and dynamics are well understood, so that network effects can be isolated and understood, that is less true for brain networks. There, understanding is still emerging of: node and link weight definitions, information representations, signalling dynamics, and the roles of space and time in network functions.

A brain network is spatially embedded and constrained to a finite volume. It is increasingly realised that this imposes constraints [22-24] and wiring costs [25, 26] on brain networks. Meanwhile the theory of spatial networks is available [27]. The nodes are at known geometric locations that are recorded in an Atlas [13], or as

injection site locations used in the experiments [9]. Thus Euclidean distances or fibre path lengths between network nodes need to be considered along with the topological or graph path lengths (simply the number of links or steps between nodes).

A brain network provides pathways that transmit and actively process signals. Thus network methods that relate to information theory are likely to provide biologically relevant insights, while the topological features that underlie graph theory [28] can address other questions. Other real-world networks, such as transportation hubs or social interactions, are more suited to study by the basic topological network methods. A generic starting point for studying the stochastic aspects of signal spread is a random walk on the structural network [29]. This captures multi-step and secondary pathways and, importantly, also captures the stochastic nature of the underlying processes. Beyond that better models, capturing the combined deterministic and stochastic elements, are required of the specific signalling, coding and processing mechanisms involved - as more such emerges these models can be developed and refined.

Modular decomposition methods [30] have been applied widely to brain connectivity data [1, 5] and show local clusters that are more densely inter-connected than the overall network. It has long been anticipated [31] that such modules may be hierarchically organised [32] in biological systems. It also should be borne in mind that network analysis methods commonly applied to brain data often are based on graph theory methods that rely on topological shortest paths between nodes. In a brain network that is spatially embedded, weighted and directed, and that transports and processes information, it is likely that multiple and secondary paths may contribute additional routes between nodes [33]. Random walk based methods can incorporate such multiple paths and may yield more biologically relevant modules. It also has been pointed out that plausible modular decompositions can be affected by: artefacts of discretization, threshold choice, algorithm choice, or simple ordering of nodes [15, 34]. Additionally, tree or dendrogram based methods that use correlation measures applied at a chosen cut-off level can guarantee that a hierarchy will be found.

Time dependence enters in at least two ways: the network structure may change: synapses strengthen or weaken over time, so that the link weights change; or new links may be formed or existing ones pruned. That may be relevant during development or learning, but not for sensory signalling. The methods of time-dependent networks [35] can be used to study those phenomena. In a brain signals travel over specific axons, the network links, at a constant velocity that also may vary with axon diameter and myelination (cf. Methods). Recent developments in the theory of temporal processes on networks [36, 37] provides methods to study spreading phenomena, including signalling, on such networks. In particular, not all linked nodes may be reachable within a given time frame. Just as in special relativity, where light carries signals at a constant speed, only some regions in space are reachable within a given time: there is a “space-time cone” which contains physically reachable targets [38]. Similarly in a network of spatially embedded axons and synapses not all network links will be relevant to a specific signalling pathway. Signals, carried by action potentials, spread out across the next available links in an ordered sequence, or “time-respecting paths” [36, 37]. Some nodes, although linked, may not be reachable within a specified time over the available sequence of traversed links. Additionally synapses incur a short delay in the propagation sequence, and also

offer the opportunity for integration of multiple incoming signals, as well as coincidence detection. Thus some network nodes may be reachable by multiple signals that happen to arrive within a small time window, so they are available for co-incidence detection and integration [39]. Other studies have used event-related networks to characterise the time evolution of brain functional connectivity [40]. Finally modular structure of the network may have some time dependence, given that links are instantiated over the signalling time-of-flight. Thus module features may evolve from an initial, local structure formed by short links to the steady state structure that includes longer, possibly brain wide, links. Separate again are representations of space and time in the brain [41], of relevance to navigation and memory: such are not considered here.

While simple network theory provides some descriptions of the mouse brain connectome it has limited ability to reveal useful insights unless the network measures can capture the relevant underlying processes, such as time dependent information flows on a spatially embedded network. It is the combination of data analytics, network analysis, visualisation and process modelling that can reveal biologically relevant insights. The research strategy adopted herein, involving network analysis methods, algorithm and software choice, and 3D visualisation methods, were laid out and tested on the mouse retina connectivity data [11].

Many experimental studies of brain circuits rely on targeted experimental probes to reveal specific circuit pathways: there are many structural network links available, but not all may be functionally activated in a given situation. The disparity between functional and structural probes of brain connectivity highlights the challenge. Here, network methods can identify, or confirm, important signalling pathways in the brain such as the primary sensory routes, along with multiple secondary links to other sensory modalities and to cortical association areas. It is possible to explore the locations and timing of integration of signals from multiple senses and so explore sensory integration. Ultimately richer network models encompassing multiple network layers, signed links describing excitation and inhibition, spatial embedding, time dependence, and link activation mechanisms, may yield real theoretical insights into brain circuits and networks.

The present study integrates the methods described above to elicit biologically relevant features of the mouse brain network structure. It focuses on information flows on the network, rather than graph methods based only on shortest paths.
This paper: analyses the mesoscale mouse brain connectome, comprising weighted directed links; focuses on ipsi-lateral connections only; analyses the connectivity data by thresholding and sensitivity analysis; incorporates a spatially embedded and temporal network; employs a range network measures to identify key nodes and links; finds the network modules using the infomap method; and presents 3D layouts of network features in both the Allen Atlas coordinates and in a simplified schematic layout. It also probes the network by tracing primary sensory signalling pathways embodied in the network, and by examining integration of signals between the association areas of the mouse cortex. More detailed network features are presented in the supplementary figures, with biologically relevant results in the main text.

Results

Connectivity strength versus distance

The links weights used here are the original normalized projection strength [9] (cf. S1 Figure) suitably normalised to a unit value (cf. Methods). Figure 1 presents the link weight vs. distance data (cf. Methods) as a log-linear plot, omitting the 10 extremely low points in S1 Figure, and with the link density normalised by a nominal threshold value of $10^{-3.5}$ (mm^{-3}) [9], taken as a unit weight. This link weight is dimensionless (i.e. unit free) and embodies a credible unit weight. A linear fit to the data in the log10-linear plot shows the distance trend and the significant dispersion in the data. Using a kernel regression model to infer voxel level connectivity [42] also found a linear trend for the whole brain ipsi-lateral data, with a log(weight) - log(distance) slope of -3.16, and residuals best fit by a log-normal distribution. Note that the comparable log-log fit to the data in Figure 1 yields a slope of -2.42, with R^2=0.18 and 95% confidence interval of [-2.49, -2.34].

Figure 1. Link weights vs. distance. Normalised link weights, plotted as $\log_{10}$(weight) vs. link distance; and log-linear fit trend (black solid line) fit by the equation $\log_{10}(\text{weight}) = 2.509 - 0.293 * \text{dist}_{(mm)}$ with R^2=0.20; 95% confidence interval for the slope is [-0.307, -0.289]. Also shown are: the 3-sigma lines (red, dashed), the unit weight (i.e. $\log_{10}$(weight) = 0, green dashed line) and the top 40% (gray dashed line) cut-off values.

In human brain the trend, over 200 mm, was fit by a quadratic [43]. For mouse, with smaller distances ~ 12 mm, a linear fit suffices, with any quadratic term making a negligible (<2%) contribution. De-trending the data, by subtracting out the linear fit, shows that the residual log-weights appear to be skew-normally distributed (Matlab dfittool) about the local mean values (now zero at each distance), with overall standard deviation 1.31. Longer links (>5mm) show slightly more dispersion (standard deviation of 1.4, vs. 1.13) than shorter links (<5mm). This is in contrast to the larger difference noted for human brain over the much longer distances, where the dispersion of log-weights increased with link distance.

Figure 1 also shows the local data mean (the linear trend line) and the 3-sigma trend lines (cf. Methods for the correct sigma of log transformed data). Often in data analysis points lying beyond the 3 standard deviations are omitted as outliers. Here 46 data points lie below the lower 3-sigma line so could be omitted as statistical outliers. Note this criterion now depends on link distance, so some care is required in eliminating weak connections. It is now clear that most of the data lies within the 3-sigma curves. Note that the strongest In-link, to CP (Caudoputamen), which appears to be an outlier, does lie within the local 3-sigma boundary. This node is also by far the largest sampled anatomical region. That makes it problematic to normalise the links to the strongest weight so that the normalised weights vary between 0 and 1, as is often used.

Figure 1 plots two credible link cut-off strengths: at weight 1 (corresponding to Oh's [9] normalised projection strength of $10^{-3.5}$ mm^{-3}), and the top 40% of link weights, as

discussed below. The plot now makes it evident that a simple threshold discards data in a skewed manner, with shorter stronger links preferentially included. More of the longer weaker links are discarded with a uniform cut-off. Possible roles of such weak links bears further investigation, as presented below. Recent study showed that the links across distance scales can have a role in global synchronization, based on a coupled oscillator model [44]. Choosing only the top 40% of structural links, consistent with ROC (cf. Methods) analysis [9, 45-47] and comparisons with functional data [45-47], discards a majority of the structural data. It does however reduce the risk of including non-functional links and aids the analysis and visualisation.

Adjacency Matrix

The raw connectivity, or adjacency, matrix normalised as described above contained 16,954 entries. These include 90 connections that returned to the source region. Thus there are 16,864 directed links between the 213 separate regions: 38% of all possible links. The 90 self-loops would constitute diagonal elements in the adjacency matrix. In network terms these self loops are links that are traced from a source region/node back to itself. Given that some regions have large voxel counts it is to be expected that sub-regions may connect between themselves. However, at the resolution of mesoscale connectivity, no further information is available. Theory shows that these self-loops can be significant in functional correlation matrices [15]. Most network analysis ignores such "return to source" links, and they are ignored in the present analysis. Numerical values of the adjacency matrix are presented in S1 Data.

Subsequent analysis generally uses only links with strengths above such a chosen threshold. Here we follow the choices made in the earlier [9, 16] analysis of the mouse data, and in light of further comparisons to MRI data [44-47]. The initial analysis [9] utilises an effective cut-off strength of $10^{-3.5}$ (mm^3), or approximately 1/3 of a voxel volume. This neglects the weaker 2762 structural links. That cut-off was also used to re-scale the link weights. Thus the weakest remaining link was assigned weight 1, so then the strongest link has weight 64.5k. The significance and possible roles of the weaker putative links is examined separately below.

Networks characteristics

Some basic features of the mouse mesoscale connectome have been reported already [9, 16]. The weighted degree (often called node "strength") is the sum of the weights of either in and out links, being the column sum and row sum, respectively, of the weighted adjacency matrix. These quantities can be calculated directly from the published Allen data [9]. They span 5 orders of magnitude, as reported previously [9, 16]. S2a Figure shows the distribution of the weighted in- and out-degree (strength) of the 213 anatomical regions (nodes). The distribution is heavy tailed, but with only 15 nodes having a weighted degree (in or out) greater than 10,000. In that case the mode (middle value) is a more robust estimator of representative links weights than the mean, which is unduly influenced by the larger values. The link weights have mode values of 264 (in) and 79 (out), both significantly below the strongest link weights. One node (#36, CP) has a very large weighted in-degree (64k) and might almost be considered an outlier in the statistical sense, being near 3 standard deviations above the local mean. It also represent a quite large anatomical region, comprising 24k voxels with an indicated geometric extend of approximately 3 mm. It also is a significant outlier in a plot of wt- in-degree vs. number of in- links (not shown).

The unweighted node degree – of the binarised adjacency matrix – counts the number of links, regardless of weight. In particular, k_i^{out} the number of Out-links from a source region is used in Methods. The distributions of unweighted degree are presented in S2b Figure. The mean number of both in- and out-links is 80, with nodes having between 3 and 180 Out-links, and between 50 and 120 In-links. Interestingly both link count distributions appear to be nearly Gaussian, with the out-distribution more skewed to the right. This suggests the speculation, in light of the Central Limit Theorem, that links might originate from a process having multiple random features, with link weights subsequently developing by more specific biological mechanisms. At the mesoscale resolution, with 213 nodes, there are not enough data points to distinguish if the degree distribution is exponential or a power law.

S3a Figure shows the distribution of graph shortest paths for the full network. These are the shortest path length (number of links traversed) between any two nodes. In a graph theoretic sense the network is compact: approximately one third (31%) of node pairs are separated by one link, with the balance (68%) reachable by two links; a very small number (232 pairs) require 3 links. Any node can be reached from any other in at most 3 links. As noted the brain network is embedded in the geometric space enclosed by the skull. S3b Figure shows the distribution of link lengths in geometric space: it appears to be a normal distribution, skewed to the right. The peak shows the most probable link length is short ranged: around 3-4 mm, while the long tail to the right shows a still significant number of very long links (~10 mm), almost spanning the full brain.

Other network measures used to identify key nodes include: node Betweenness Centrality (BC) and edge BC [6, 28], which count the number of shortest paths that traverse a node or link in the network. For signalling networks random walk centrality [33] and probability flow (essentially frequency of random walk visits, as counted by the InfoMap algorithm) [48, 49] may also be of value. S1 Table presents the top 20 nodes rank by probability flow and lists other network measures. These nodes are most frequently visited by a random walk on the network. Many have high degree and number of linked (i.e. un-weighted degree). Some, but not all, have high nBC. S2 Data lists all nodes with detailed information and network measures.

Analysis of complex metabolic networks has generated the concept of hub nodes [50, 51], based on the participation coefficient, P which measures the diversity of a node's out links to other network modules (see below). More than half of the mouse brain nodes (113 out of 213) have $P > 0.5$ (within a range 0 - 1), indicating some hub-like character. Of these, five nodes also have very high weighted In-degree and random walk flows; while six nodes have very high weighted Out-degree. Together these measures may help to identify connector hubs. Likely hub nodes are listed in S2 Table. Such hubs often are evident in the Figures. Amongst the high participation coefficient nodes are 21 cortical regions, including most of the association areas, the visual and auditory cortices, and the secondary motor region. Three way comparisons of probability flow and participation coefficient to both In- and Out-Degree (figures not shown; cf. S2 Table and S2 Data), are informative. A few nodes (MRN, PAG, SCm, LHA, ACB) stand out by having high flow, with many others clustered near low flow and degree. Participation coefficient highlights other nodes (eg. CLA, CLI, PP, GPi, MGd, MOs, ENTl) and tends to spread nodes out more evenly. In each case

CP is possibly an outlier due to it being the largest sampled anatomical region. A similar comparison using node BC is less informative since more nodes are clustered near zero. Overall it appears that these standard network measures, applied at this spatial resolution, provide only a partial guide to functional significance.

Modules

Modular decomposition of the mouse connectome, via its adjacency matrix, was attempted by the usual variety of methods: spectral partition of the Laplacian matrix and of the modularity matrix, k-means, agglomerative and divisive methods [52- 54] and the Louvain method [55] which iteratively agglomerates nodes. Many of these methods rely on network topology measures (node BC, edge BC) that reflect shortest paths on the topological network. The InfoMap algorithm [48, 49], by contrast, uses information theoretic concepts (Hoffman code length) as a proxy for random walks on the network [48], so may be more appropriate for a brain network. It also does not require the number of expected modules to be specified in advance - that emerges naturally from the calculation. Such random walk based methods allow link weights and secondary pathways for information spread to be included. The results presented below all use the InfoMap method applied to all 14,103 links of weight 1 or larger (cf. Figure 1).

Ranking of nodes in order of probability flow correlates well with random walk centrality and weighted in-degree (cf. S1, S2 Tables), or node strength. Clearly that reflects the algorithm design. However such ranking does not correlate well with shortest paths node BC, with the latter likely dominated by numerous long-range weak links. The Infomap calculations were robust to the choice of filtering (cut-off) of link weights: cut-off weights of 1, 78 (top 40% of links), 0.1 and 0.01 produced either identical results (for 1, 78) or only minor differences (for 0.1, 0.01), suggesting that the modular decomposition is robust. In all cases the major modules and their leading (i.e. highest flow) nodes were identical.

Figure 2 shows a comparison of the mouse brain anatomical regions and the calculated network modules. The regions are represented by the 3D convex hull surface that encloses all member nodes, plotted in the Allen Atlas coordinates. Note that the convex hull encloses the node coordinates that are the centroid coordinates of the anatomical region, rather than covering the full extent of those regions. Thus the region-enclosing surfaces are not space filling: this improves the visibility of the 3D graphic. Surface colours match those presented in the Allen Brain Atlas sagittal slice images [13+]. The modules are presented in 2D only to reduce confusion in the image. Modules are represented by the 2D slice of the convex hull (enclosing all module members) drawn at a height (in the Dorsal-Ventral axis) corresponding to the centre of mass (CM) of the module members. Note that there is significant, but incomplete, correspondence between modules and the major anatomical regions. Overall 74% of all links are between modules, with mean length 4.3 mm, while 26% are within modules, with mean length 2.8 mm.

Figure 2. Network modules and brain regions. 3D plot of mouse brain major anatomical regions, drawn as a translucent convex hull enclosing centroids of member anatomical regions; and Infomap modules, enscribed in 2D (at height (ventral-dorsal axis) of the CM of nodes). Region colors are taken from the Allen Atlas sagittal

images [92]; module colors follow that of the dominant members. Bregma is marked by the cross. A mid-level horizontal slice through the 3D Nissal stain image [13] gives perspective. A 1 mm scale bar is shown on that mid-slice. A floor grid of 1 mm squares is drawn at 6.7 mm ventral to Bregma to give further 3D perspective.

Table 1 lists the Infomap modules and their key characteristics, (cf. S2 and S3 Data for full details). Module 1 is the largest and mostly contains anatomical regions from the hind brain (medullla, pons, cerebellum) along with some (27%) from the midbrain. Module 2 is dominated by cortical (motor, somatosensory) and thalamic regions; it also contains CP, the largest and most densely connected region. Module 3 is mostly associated with the hypothalamus, along with the striatum and thalamus. Module 4 is dominated by the olfactory regions in two broad locations: anterior (MOB, AOB, AON, TT) and posterior to Bregma (PIR, COA, NLOT, PAA, TR); it includes the perirhinal region. Thus this module has a significant spatial extent in Figure 2. Module 5 contains the auditory and visual regions of the cortex, along with their thalamic pathways (LGd, MGd); it also contains the nearby, posterior cortical association areas (parietal, retrosplenial, temporal). Module 6 is dominated by the hippocampal formation, along with some elements of the palladium and striatum. Module 7 contained the anterior cortical regions (orbital, limbic, insular, cingulate) along with the claustrum and five nearby thalamic regions (AMv-d, SMT, MD, CL). Module 8 is dominated by the cerebellum. In each case a small number of nodes in other regions are well connected with the main elements of each module - so there is not a complete alignment between regions and network modules. Three regions (FS, MH, RH) appeared as "orphans" not assigned to any module – judging by their dominant linkages they appeared to be related to Module 1, so were assigned there for convenience. Modules were color coded by their dominant regional members. In subsequent figures nodes and links are colored according to their module membership, as described above.

Module	Flow in Module	Key regions	Anatomical Regions	Color
1	0.321	MRN, PAG, SCm	Midbrain, Pons, Medulla	pink
2	0.229	CP, SNr, GPe, Mop, SSp, SSs	Striatum, Thalamus, Cortex	mid green
3	0.159	LHA, SI, ACB	Hypothalamus, Palladium, Striatum	red
4	0.102	MOB, AON, PIR, ENTl	Olfactory	olive green
5	0.068	Vis, Aud, TEa, LGd, MGd	Cortex, Thalamus	dark green
6	0.058	CA1,2,3, DG	Hippocampus	light green
7	0.038	ACA, ILA, AIv, ORB, CLA	Cortex, Thalamus, Cortical Subplate	salmon
8	0.022	AN, SIM	Cerebrum	yellow
orphans	0.003	FS, RH, MH	Pons, Thalamus	n/a

Table 1. Informap modules for mouse brain ipsi-lateral regions and links. Key members, in order of probability flow, and color coding used in the figures are listed.

Functional roles associated with these modules emerge from analysis of sensory and association pathways, presented below. This accords with other findings of modules that broadly align with anatomical regions [56] (and cf. Fig. 2). The modular decomposition found also approximately aligns with the four system model [57], that divides the brain into four functional systems: sensory, motor, cognitive, and behavioural state. Network modules 2, 4 and 5 handle sensory roles; module 2 also contains the motor roles, modules 2 and 5 contain the cortical association areas, and modules 1, 3, 6 and 8 relate to behavioural state. A key nodes (e.g. CLA, ENTl) appearing as linkage hubs between modules.

Other modular decompositions are compared in S3 Table. The Newman modularity metrics [52, 53] are: Q=0.40 (Infomap), Q=0.395 (Louvain) and Q=0.30 (Newman spectral). The Louvain method produces 6 modules for the whole brain. The Infomap modules 4 (Olf), 1 (Mid- and Hind-brain) and 8 (Cerebrum) are combined together into the Louvain module 1. The Louvain results substantially overlap with those of the Infomap method, with notable differences, as listed in S3 Table). The Newman spectral partition, by definition, produces only 2 modules, essentially dividing the brain into sensory + motor + cortex and hindbrain. Thus, at a gross level, the three methods are in accordance. Other Newman methods did not produce satisfactory results, either yielding only one large module, or very unbalanced divisions.

Sub-modules were investigated as stand alone systems, to see if further sub-divisions could be extracted. In particular the Infomap module #5 was investigated, since it combined the Auditory and Visual systems, in contrast to the Louvain method, where they are separated. It did not reveal further partitions. Infomap module #1, however, did subdivide, into groupings of Midbrain, Pons and Medulla.

A recent analysis of additional mouse connectivity, at the layer level of the cortex [14], used the Louvain method for modular decomposition. It found 6 modules with some similarities and notable differences to the present results. The 6 modules were described as: prefrontal (FRP, ACA, ILA, ORB, MOs); antereolateral (GU, VISC, AI-d, -p, -v); Somato-motor (SSp-m, -n, -bfd, -ul, -ll, -tr, MOp); Visual (Vis-p, -l, -al, -pl); medial (Vis-am, -pm, RSP); and temporal (AUD, TEa, PERI, ECT). Four of the 8 Infomap modules (1, 3, 4, 6, 8) found herein encompass hind- and mid-brain regions along with the olfactory regions; of these module 1 includes PERI. Three modules are associated with cortical regions: module 2 (ACA, ILA, ORB, all SSp, SSs), module 5 (AUD, VIS, VISC, RSP, TEa), and module 7 (ACA, AI-v, ILA, ORB). Notable differences in the present work are that: the frontal pole, insular regions and GU are together in Infomap module 2, comprising somato-sensory and motor regions; here MOs and MOp are in this same module. The AUD, VIS and VISC regions come together in module 5, along with TEa, ECT, RSP. In the present study the whole brain connectome was decomposed into modules. Thus nodes and modules are more inter-linked, including via extra-cortical regions. Whereas higher resolution, at the cortical layer level [14], may have facilitated decoupling of auditory and visual regions.

All calculations of modules based on the full adjacency matrix, independently of cut-off weight assumed, produced a two-level decomposition – that is, no hierarchy was detected. That also was found for the mouse retina microscopic connectivity data [11]. However examination of a distance-sliced adjacency matrix did reveal an

evolution of hierarchy, which was evident for closely spaced nodes whose links activate early in signalling pathways. Progressive inclusion of longer range links washes out that hierarchy, which is swamped by denser interconnections formed at later times, or equivalently longer link distances. In that calculation links are activated sequentially over transit times, or equivalently link distances. Those results are described below (cf. Fig S9), after the effects of link length are discussed.

Network Visualization

With the basic network characterisation in hand it is now possible to show the overall network linkage patterns. S4 Figure shows all 213 anatomical regions as network nodes plotted in 3D at the Centroid (mean coordinates) in the Allen Atlas coordinate space, along with all their Out-links. Nodes are coloured by their module membership and links by the module membership of their target. However a plot of all nodes and their In-links is not discernibly different, despite the differing Out- and In-degree patterns (cf. S2 Figure). Overall linkage patterns, as reflected by the link colors, appear to correspond with brain regions. This is consistent with Figure 2, which shows significant overlapping of network modules with anatomical regions. While there are difference in the patterns of Out- and In-links such cannot be immediately discerned in these images. This immediately highlights the basic challenge that is usually encountered in network visualization: the fabric of links is too dense to discern more than the overall pattern. In particular there are too many links crossings that occlude other features in the 3D fabric of nodes and links. As with experimental investigations of brain networks, a subset of nodes and links needs to be targeted to discern details of regions and circuits.

Here four strategies are adopted to make progress: network nodes are placed at simplified schematic coordinates (cf. Methods, S3 Data and S10 Figure), which will serve to reduce the number of link crossings and so reduce visual complexity; a number of landmark nodes are examined (e.g. high In- or Out-degree, high flow, or hub nodes); and links are selected from either the strongest (e.g. top 40%) or weakest present; next functionally relevant pathways may be examined, such as the primary sensory paths, or inputs to and outputs from the cortical association areas; or links with the motor regions. The latter approaches are informed by the many experimental probes that follow the primary sensory and association cortex pathways. These, historically, have produced basic insights into nervous system and brain function [58]. Similarly network methods allow computational probes of links to, and from, key sensory and cortical regions.

Figure 3 shows all nodes and the strongest 40% of ipsi-lateral Out- and In-links (5,641 links in total) with all 213 nodes, now plotted in the simplified schematic coordinates. Overall there is a reciprocal pattern of links between major regions. Cortical association areas, including the ventral olfactory region (PIR), along with motor and selected midbrain regions, are significant integration hubs. From the color coding of links it appears that many of these are hubs with their relevant module (e.g. Frontal Pole, Orbital, Insular), while others are integrating between several modules (e.g. Cingulate, Temporal, Parietal, Retrosplenial) or across several senses (Aud, Vis, Olf). Closer examination reveals mutual, strong (i.e. top 40%) links between somatosensory regions and both auditory and visual regions, with the temporal, parietal and cingulate regions having strong in-links from auditory and somatosensory regions. The retrosplenial region receives inputs from the gustatory, visceral and

visual senses. The orbital, limbic and cingulated regions have strong In-links from the olfactory and auditory senses. The somatosensory, gustatory, visceral, auditory and visual primary senses all link directly to the motor regions. There is no direct link from the primary olfactory regions (AOB, AON, MOB) to either MOs or MOp. Possible weaker links are examined later. It is evident that a further strategy is required to unravel the complexity of links evident in Figure 3.

Figure 3. 3D schematic coordinates for mouse brain. All network nodes plotted in 3D schematic coordinates (cf. S10 Figure and S3 Data), along with the top 40% of links: **a**. Out links and **b**. In links. Anatomical regions outlined as in Figure 2. Only the right hemisphere and ipsi-lateral links are shown. Out-links are colored according to the module of their target (cf. Table 1), and In-links according to their source module. Other details as in Figure 2.

Unfolding of links in sensory pathways

The network analysis present thus far considers of the linkages patterns and their spatial separation, and ignores time. That is they present the long time, steady state behaviour of the network of nodes and links. Now we examine the unfolding activation of those links through time, or over distance. The results presented above relate to nearest neighbour links, over one step, between nodes. Recalling S3a Figure it is clear that many node pairs are separated by 2 steps over the network. Likewise Figure 3b suggests that, for a given signal velocity over axons, two shorter links can be traversed in the time window for one long link to be traversed. It is also evident from Figure 1 and S1 Figure that shorter links tend, on average, to be stronger than longer links. Thus it may be useful to examine the evolution of links over major sensory pathways.

Figure 4 shows the top 40% of out- and in-links from/to key primary sensory regions: Visual (-p, -al, -am, -l, -pl, -pm), Auditory (-d –p –v), SSp (-bfd, -n, -m, ul, tr, ll), Olfactory (MOB, AOB, AON) and Gustatory + Visceral, 20 source nodes in all. Here only ipsi-lateral links are described. These links are shown in two ranges of link, or equivalently signal time, windows: $d < 5$ mm (Figure 4a) and $5 < d < 10$ mm (Figure 4b). The first set is equivalent to about half the brain size, being the approximate width of one hemisphere or half its length; the second almost spans the full size – in the present case no longer links of high weight were present. The 20 source nodes together have 530 high weigh direct links (top 40%): of these 426, or 80%, have link distance $d < 5$ mm while 104 are longer range, up to 10 mm. Two-step links begin to appear for $d > 3$ mm, or equivalently $t > 3$ msec; in the short interval ($d < 5$ mm) 204 such structural links are present. Of those possibly only a fraction are activated to functional roles. The second window (5-10 mm links) contains the remaining 15,367 two-step structural links from the combined 20 source nodes. The images superimpose many such links given the common structural coordinates assigned to nodes so many details are masked. Even so, some integrative features emerge: there is a clear anterior-posterior localization of processing on shorter time scales.

Figure 4. Primary sensory pathways. Major sensory pathways, shown by strong Out-links (top 40%) from 20 primary sensory areas (listed in text) plotted in schematic coordinates: **a**. link distances, $d < 5$mm and **b**. $5 < d < 10$mm. Nodes are

colored by their module membership, and links by the module membership of the target node.

Shorter links (Figure 4a) carry sensory signals to nearby association areas, e.g. Olfactory (Olf) to the nearby Limbic and Orbital regions, and then later to PIR and TT; Somatosensory (SS) regions output directly to Motor, Limbic, Orbital and Cingulate regions, along with the dorsal Striatum and the Gustatory/Visceral (GU/Visc) regions. Auditory output is direct to Temporal and Parietal regions, and also to Visual regions (Aud-d to Vis-l, -am, -pm; Aud-v to Vis-al, -am; Aud-p to Vis-p). Visual output is direct to both Parietal (from Vis-p and Vis-am) and Retrosplenial (from Vis-am) regions. Both Auditory and Visual primary regions link directly to selected Somatosensory regions (Aud-d, -v to SSp-bfd; Aud-d, -p, -v to SSp-tr; Aud-d, -p to SSp-ll; and Aud-d to SSs).

Cross modal linkages are evident. Both Visual and Auditory outputs have close – i.e. fast acting – and strong cross linkages: Vis-l to Aud-d & -p (d < 2mm, weights 1185, 630 respectively), Vis-am to Aud-d (d < 3mm, weight 150); and Aud-d to Vis-p (d < 2mm, weight 845), Aud-v to Vis-al (d < 2.5mm, weight 790) and Aud-p to Vis-am (d < 4mm, weight 330). Both Auditory and Visual outputs also return to regions in the Midbrain (to Ic-e, -d, SCm and to SC-s, -m respectively). GU/Visc regions link to SS-s and the Insular, Temporal and Parietal regions, and also, less strongly, to the Hypothalamus (LHA); GU alone also links to SSp-bfd, -m while Visc alone links to SSp-bfd, -m, to SSs, to MOs and to the olfactory region PIR. Olf, multiple Somatosensory and GU/Visc links converge to CP, along with Auditory inputs. Visual inputs are not direct, but rather via Parietal and RSP regions. Somatosensory and GU/Visc regions link to the posterior association areas, with the latter also interacting with the ventral Olfactory region (PIR); also note that SS links to the Retrosplenial region, while GU/Visc links to Parietal. The GU/Visc regions link directly to: Auditory (GU to Aud-p, -v), to Somatosensory (GU to SSp-m; Visc to SSp-tr, -ll, SSs), Visual (GU to Vis-p, -am; Visc to Vis-p, -l, -pm, -pl) regions, and to the Cortical Subplate (Claustrum). At this long distance the Frontal Pole only receives strong input from the Orbital association area. Overall most interactions are within module.

At longer times (corresponding to longer links in Figure 4b) anterior-posterior coordination emerges; there is more between-module interactions and cross-talk between cortical association areas. The Parietal and Retrosplenial regions link to multiple regions of the Midbrain; and many regions now link to ventral and hind brain regions. Olfactory outputs travel via PIR to the temporal cortex, to GU/Visc, to one amygdilar region (COAa) and ventral regions: Hippocampus (CA1), Cortical Subplate, Striatum and Palladium.

From the 3D images a number of regions emerge as apparent network hubs, sending or receiving multiple links between sensory modalities or between modules (indicated by link colors). Note that such regions were not immediately identified by the network "hub" measure, suggesting that a combination of techniques may be required to dissect key nodes and links. These emerge at link lengths, 5 < d < 6.5 mm, and most are in the Olfactory system, with each having ~20-45 In-links in the top 40% of links. S5 Figure show these links in two distance (or, equivalently, time) slices. The 5 target hubs are: ACB (nucleus acumbens, Striatum) with very strong (weight > 10k)

In-links from the Insular region (AIv), Thalamus (PT, IMD), Cortical Subplate (BLA) and Midbrain (CLI) – here source nodes are listed by increasing distance from the target. The next hub-like target is the endopiriform nucleus (EPd, Cortical Subplate) with medium strength (weight > 1.5k) In-links from the Cortical Subplate (CLA, BLA), Isocortex (AIv, PERI), Olf (PAA, TT) and Midbrain (CLI). The caudoputamen (CP, Striatum) is the largest sampled region [9] and likely in consequence has a large number (72, cf. S2b Figure) of strong In-links. The strongest link in the connectome is from the Frontal Pole to CP (weight 64k). Other very strong links (weight > 10k) are from the Cortical Subplate (BLA), the Isocortex (PERI, ACAd), Thalamus (AMd, PF, CM) and Midbrain (SNc, CLI). The next suggested hub is the dorsal peduncular region (DP, Olf) has only relatively weak (weight < 500) inputs, the strongest of which are from the Thalamus and PERI. Next is the postsubiculum (POST, Hippocampus) with modest (weight > 500) links in locally from SUBd, and then from Midbrain (NOT), the Retrosplenial region (RSPv), Thalamus (AD, AV) and Cortical Subplate (Claustrum). The perirhinal region (PERI, Isocortex) has medium (weight > 1k) links in from the Cortical Subplate (LA, CLA), Olf (PAA) and Thalamus (SMT, SPFm), along with a weaker (weight 556) input from the frontal pole.

PERI is noteworthy in having numerous, diverse and strong outputs to 7 of the 12 major anatomical regions, along with feedback to some senses (SSp-n, -m, -bfd, tr and AUDd), along with a weak link (weight 100) to the frontal pole. The other "hub" nodes discussed have relatively fewer (~ 10-30) and weaker Out-links. EPd is notable: it strongly links (weight 4.7k) to ENTl – that, along with ACB, were identified as hubs via the participation coefficient (cf. S2 Table).

Fabric of Weak Links

Figure 1 shows a strong fall off of link strength with distance: selection of the top 40% of links, while avoiding false positives, also omits some potentially important weak links. Suggestions that weakest links may have other characteristics or roles, such as stabilising complex networks [59] suggest that weaker links should not be ignored even at the risk of including false positives. Now we examine the fabric of weak links out from the primary senses, specifically the 20 nodes examined in Figure 4. Recalling Figure 1, there are 2751 links with weight < 1 (and > 10^{-6}, the weakest included herein); of there 369 links emerge from the 20 primary sensory nodes. As with S5 Figure, it is illustrative to separate links into short range (reached in shorter time) and longer range: 25% of such links have length < 5 mm, while 62% are < 6.5 mm. By contrast 80% of the strong links (Fig 4) have length < 5 mm. In the following links are listed in order of increasing distance, with shorter first. S6 Figure shows these weak links in the two distance, or equivalently time, windows. S6a Figure shows the shorter (d < 6.5 mm) weak links: note that, in contrast to the strong links, they do not target the motor regions or most of the cortical association areas. Only Cingulate and Retrosplenial regions have a few weak In-links. All weak links, up to length < 10 mm, are displayed in S6b Figure. Now there are multiple long-ranged feedback links to the Cingulate and Retrosplenial regions, and a number of possible two-step links to Motor regions: 111 into MOp: e.g. MOs – prelimbic – MOp, MOs – Cingulate (ACAv) – MOp, SSp-m – STN – MOp, etc; and 128 into MOs: eg. AON – TRS – MOs, SSp-n – TRN – MOs, MOB – TRN – MOs, etc. It is unknown which, if any, of these very weak structural links are functional. There are no one-step weak links into MOp or MOs. Otherwise most Out-links from the primary sensory regions are to the behavioural state system (in Cajal's classification [57]), the hind brain,

thalamus, hypothalamus, and hippocampus, along with the midbrain and ventral olfactory regions. There are also 15 very long range (10 < d < 12 mm) weak links (not shown), the majority from MOB, the most anterior anatomical region.

Cortical Association Areas and Sensory Integration

The combination of network analysis and visualization also permits examination of concurrent In- and Out-links to the cortical association areas. The separation of the Isocortex into anterior (Somatosensory-Motor) and posterior (Auditory-Visual) modules (Figure 2) suggests examination of the two regions separately. The four anterior association areas: Insular, Limbic, Orbital and Cingulate are shown in Figure 5. At first sight the In- and Out-links appear to be symmetric. However, closer examination reveals detailed differences. In total there are 354 strong (top 40%) In-links (Figure 5a) to these four regions; sensory inputs are listed first. Orbital regions receive sensory inputs: ORB-l from AON, weight 190; ORB-l, -vl from SSp-ll, weights 90, 125; ORB-vl from SSp-bfd, -tr, weights 135, 115; ORB-vl from VISC, weight 545. Longer range inputs are: ORB-l, -vl, -m from AUD-v, weights 330, 265, 115; and ORB-vl from Vis-l, weight 415. Limbic regions receive inputs: ILA from AON, weight, 175; PL from SSp-ll, weight 105; PL and ILA from VISC, weights 140, 245; PL and ILA from Vis-l, weights 80, 340; ILA from AUD-v, weight 245. Insular regions receive inputs: AI-d, -p from GU, weights 1.2k, 300; AI-v, -p from SSp-n, both weights 95; AIp from SSp-m, weight 110; AId from AUD-v, weight 220; AId from VISal, weight 295. Cingulate regions receive inputs: ACA-d, -v from SSp-ll, weights 425, 85; ACAd from SSp-tr, weight 255; ACAd from SSp-bfd, weight 85; ACAv from GU and VISC, weights 135, 770; ACAv from VISp, weight 215; ACA-d, -v from VIS-l, weight, 295, 335; and ACAd from AUDv, weight 90. AId has a very strong input (weight 13k) from the Frontal Pole, with weaker inputs from AIv (weight 1.2k), AIp (weight 678) and the prelimbic region (weight 1.4k) to FRP. Overall these association areas share the inputs from the more anterior senses, and also have lesser inputs from the posterior senses: AUD and VIS. There are also inputs from the posterior association areas: ORB-l, -vl from PTLp, weights 200, 480; ACA-d, -v from PTLp, weights 865, 460; ILA and PL from PTLp, weights 250, 145; ILA from RSPv, weight 140; ORBl from TEa, weight, 80; AId from TEa, weight 275. All these anterior regions receive strong (weights ~1k - 2k) structural links from the Claustrum, as found by other tracer studies of the mouse neocortex [55].

Figure 5. Anterior cortical association areas. **a**. Strong In-links to anterior cortical association areas (Limbic, Orbital, Insular and Cingulate). Only direct (first nearest neighbour) links are shown for clarity. Stronger or multiple links are highlighter by thicker lines. **b**. Strong Out-links.

There also are 399 strong (i.e. top 40% by weight) Out-links (Figure 5b) from these four regions. Again these are shorter range links, with 70-80% being less than 5mm, and the most probable link length is 2.5-3.5 mm. There are numerous strong local links between the four anterior association areas; all connect to the Motor regions (AIv to MOs, weight 6.6k; AId to MOp, weight 1.1k; ORBl and ORBm to MOs, weights 4.5k and 1.3k, respectively; ORBvl to MOp, weight 1.1k; ACAd to MOs, weight 4.8k; ACAv to MOp, weight 500). Only ORB-l, -m connects to Frontal Pole (weights 635, 200). Feedback to sensory regions is: from Insular to Olfactory; from Limbic, Orbital and Insular to Somatosnsory regions (ILA to SSp-tr, weight 120; ORBvl to SSp-m, weight 80; ORB-l, -vl to SSp-ul, weights 100, 360; ORB-vl to

SSp-ll, weight 170; ORB-l, -vl to SSp-bfd, weights 540, 480; ORB-vl to SSp-tr, weight 340; AIp to SSp-n, -ul, weights 200, 90; AIv to SSp-tr, weight 80; ACAd to SSp-tr, weight 660); while groups of three regions feedback to Auditory and Visual regions (ILA to Vis-p, weight 300; ORB-vl, -l to Vis-p, weights 420, 100; AId to Vis-al, weight 620; ACAd to Vis-pm, -p, -l, -pl, weights 100, 2.2k, 270, 90; and ILA to Aud-d, weight 170; ORB-l to Aud-v, weight 80; AIv to Aud-v, weight 190; ACAd to Aud-d, weight 200). There are medium strength outputs to the Frontal Pole, from: ORB-l, -m, weights 635, 205; and AI-v, -d, -p, weights 1.2k, 345, 120. Longer range links are to the posterior cortical association areas: ORBvl, ACAd, ACAv to RSPagl, weights 160, 360, 520; AIp to RSPv, weight 155; AIp to RSPd, weight 85; ORBvl, ACAd to PTLp, weights 695, 3.5k; ILA, ORBvl, AIv, ACAd to TEa, weights 160, 330, 1.5k, 200; and ORBm, AIv, ACAd to ECT, weights 170, 1.8k, 360). All these anterior regions have medium strength (weights ~100-400) structural links to the Claustrum; the Out-Links are significantly weaker than the In-Links from Claustrum. Inspection of Figure 5 suggests that the In- and Out-links with anterior regions are reciprocal. However the details listed above show some differences. In particular, there are many outputs from the four regions to the Midbrain, but few inputs. The Cingulate regions have outputs to the Temporal regions, but no strong inputs. Note that the Limbic region outputs to the Motor regions but has no strong inputs from there. The Frontal Pole has strong inputs from Limbic, Insular and Cingulate Regions, but only outputs to Orbital and Insular Regions.

Links with the three posterior association areas: Temporal, Parietal and Retrosplenial are shown in Figure 6. The 216 strong (i.e. top 40% by weight) In-links are shown in Figure 6a. The figure shows that now there are longer range inputs, with temporal and retrosplenial regions having most probable links lengths of 5.5 mm, compared to 3.5 mm for the parietal region. The nearby auditory-visual regions provide immediate strong inputs: AUD-v, -d to TEa, weights 2.5k, 2.3k; AUD-d to ECT, weight 700; AUDp to PTLp, weight 805; AUD-d, -p to PTLp, weights 3.6k, 805; VIS-l to ECT, weight 2.5k; VIS-p to TEa and ECT , weights 80, 255; VIS-am to TEa, weight 630; VIS-am to ECT, weight 575; VIS-l to RSP-agl, -d, -v weight 1.1k, 2k, 550; and VIS-pl to RSP-v, weight 550. Other sensory inputs are: VISC to TEa and ECT, weights, 260, 275; VISC to PTLp, weight 3k; VISC to RSPv, weight 1.5k; VISC to RSP-agl, -d, weights 930, 1.9k; SSp-bfd to TEa and ECT, weights 405, 225; SSp-tr to TEa, weight 90; SSp-ll to both TEa, ECT, weights 235, 85; SSp-bfd, -tr, -ll to PTLp, weights 310, 730, 305. Weaker sensory inputs are AUD-v to PTLp, weight 140; VIS-am to RSP-d, -v, weight 135, 140; VIS-p to RSP-agl, -v, -d, weights 290, 215, 405; VIS-pl to RSP-d, weight 190; VIS-l to RSP-d, weight 190; GU to RSPv, weight 125; SSP-tr to RSPd, weight 85. The Temporal regions receive multiple inputs from the Hippocampus (SUBv, ENTl, ENTm, PRE, PAR, POST, SUBd). Pairs of the posterior regions receive inputs from all four anterior regions: Orbital, Insular and Cingulate to RSP and Temporal; and Limbic to PTL and Temporal regions. The Motor regions input to RSP and Temporal. There is very strong Thalmic input: MGd to TEa, weight 20.8k; and AD to RSPv, weight 31k. There are weaker, long range inputs from the Frontal Pole: to ECT, weight 295; and to TEa, weight 685; along with feedback from MOs to both ECT and TEa, weights 205, 200. Again the anterior regions receive strong structural links from the Claustrum.

Figure 6. Posterior cortical association areas. **a**. Strong In-links to posterior cortical association areas (Temporal, Parietal and Retrosplenial). Only direct (first nearest

neighbour) links are shown for clarity. Stronger or multiple links are highlighter by thicker lines. **b**. Strong Out-links.

There also are 204 strong (i.e. top 40%) Out-links (Figure 6b) from these three regions. Most are shorter range links, with 75-85% being less than 5mm, and the most probable links length being 3.0-3.5 mm. There is immediate feedback to the local sensory regions: PTLp to AUD-d –p, -v, weights 1.2k, 1.3k, 220; PTLp to VIS-l, -p, -pl, -am, -pm weights 660, 1.9k, 130, 1.8k, 580; PTLp to SSp-tr, weight 1.3k; PTLp to VISC, weight 1.8k; RSPagl to Vis-pm, weight 1k; RSPv to VIS-am, -pm, -p, weights 630, 220, 1k; RSPagl, -d to VIS-pl, weights 120, 95; RSP-d, –v to SSp-tr, weights 740, 1k; RSP–v to SSp-ll, weight 130; RSP–v to SSp-bfd, weight 270; and RSP–v, -agl, -d to VISC, weights 560, 235, 690. Both RSP-d and PTLp link to Midbrain regions: RSP-d and PTLp to SCm, weights 2.3k, 2.8k; RSP-d and PTLp to PAG, weights 945, 475; PTLp also links to numerous other Midbrain regions: SCm, SCs, Ice, ICc, APN, MRN, NPL and SNr. The three regions all have relatively weak (weights ~100-200) links to numerous Thalmic regions: notably strong links are: ECT to LD, weight 810; PTLp to LP, weight 835; RSPv to LD, weight 1.3k. RSPagl links to the Hippocampal fields CA1, CA3 with weights 175, 120. There are direct link to Motor regions: TEa to MOp and MOs, weights 760, 425; PTLp to MOp and MOs, weights 1.1k, 2k; RSP-d, -v to MOp, weights 860, 1.1k. The links to the anterior association areas are: TEa to ORB-l, weight 80; PTLp to ACA-v, -d, weights 460, 865; PTLp to ORB-l, -vl, weights 200, 480. The retrosplenial regions only have structural links to the Cingulate regions: RSPd to ACAd, weight 940 and RSPv to ACAv, weight 1.8k.

Inspection of Figure 6 suggests that the In- and Out-links to posterior regions are reciprocal. Again the details listed above show the differences. In particular, the Frontal Pole has medium strength links to the Temporal region, but only relatively weak return links (e.g. FRP to TEa, weight 37 – not shown, since not in top 40%). Similarly there are asymmetries in inputs and outputs with the Motor regions. Overall it is evident that the temporal area is a significant integration hub for sensory inputs, while the retrosplenial and parietal areas are distribution hubs to the motor areas.

The Frontal Pole is examined separately since it has more long range connections, with the most probable links length being 6.5 mm. S7a Figure shows the 53 strong (top 40%) Out-links and 17 In-links with the Frontal Pole (FRP). The closest strong inputs to FRP are from the Orbital and Insular regions, along with MOs. Other inputs are from Claustrum, Thalamus and Olfactory (NLOT) regions. There is a weaker, long range input from Aud-v. The very strong outputs from FRP are to the Insular regions (weights 13k and 27k) and Motor region, MOs (weight 22k). The strongest link in the mouse connectome appears here: FRP to Caudoputamen (weight 64k). Other medium strength outputs are to SSp-m, -ul, -n and SSs (weights 2k, 3.8k, 300, 2.5k); along with Vis-al (weight 550). There are weaker, long range links to the Temporal association areas (ECT, TEa, weights 680, 300) and the Perirhinal region (weight 550). Other output are to ventral regions: Claustrum, Striatum, Palladium, Hippocampus and Midbrain. There are only a few strong inputs to FRP, from: ORB-l, weight 635 and AIv, weight 1.2k; and Thalamus (VM, weight 600). The other 14 inputs considered are all weaker (weights ~100, 200). S7b Figure shows the weaker links (bottom 60% or weight < 78) to FRP. Such have been ignored so far, for clarity and the higher chance of either False Positives or False Negative indications of

functional links. Most weak outputs are to the Mid- and Hind-brain regions: Striatum, Hypothalamus, Hippocampus, Cortical Subplate, Midbrain along with the Thalamus. Also evident in the image is a longer range link to the Retrosplenial region, and a number of 2-step links to RSP and the Parietal region. There are noticeable, medium weight, feedback links into FRP from anterior sensory regions: Olfactory (AON) and Somatosensory (SSp-m ,-ul, -bfd, SSs). Other weak inputs are from: Palladium, Hypothalamus, Hippocampus, Midbrain, Pons and Medulla.

Motor Regions

S8 Figure show the strong (top 40%) links into the Motor regions (MOs and MOp). Many of the cortical association areas have such links into the motor regions: the Frontal Pole (FRP) has the strongest links: of weight 27k into MOs and 22k into MOp. Related close, strong inputs are from the Cingulate (ACAd to MOs, weight 4.8k; ACAv to MOp, weight 500), Orbital (ORBl to MOs, weight 4.5k; ORB-vl, -l to MOp, weights 1.1k, 1k), Insular (AI-v, -p to MOs, weights 6.6k, 800; AI-d, -p to MOp, weights 1.1k, 945) and Retrosplenial and Parietal regions (RSP-d and PTLp to MOs, weights 2.8k, 2k; RSP-v, -d to MOp, weights 1.1k, 880). Temporal input is from TEa to MOs and MOp, weights 425, 760. Direct sensory inputs are from multiple Somatosensory primary regions (SSp-ll, -tr, -ul, -bfd to MOs, weights 1.1k, 990, 845, 2k; SSp-tr, -ul, -bfd, -m, -n to MOp, weights 1.4k, 3.7k, 2.7k, 4k, 1.2k; and SSs to both MOs and MOp, weights 790, 1.6k), along with Gustatory and Visceral links to MOs (weights 1.7k, 1.4k, respectively) and to MOp (weights 4.9k, 930). There are a strong inputs from Aud-v (weights 2k, 1.4k) and Vis-am (430, 300) to both MOs and MOp; and relatively weak inputs from AUD-d to MOs only, weight 385; and AUD-p and VIS-al to to MOp only, (weights 320, 335). Olfactory input is: DP to MOp, weight 305. Note that other direct inputs from the Olfactory regions are relatively weak; rather AON links to motor regions via Orbital and Insular association areas. Hippocampal input is CA2 to MOp, weight 125. There are long range, weaker inputs from Pons and Medulla. Note that a number of weaker two-step structural links are shown, via the Restrosplenial, Cingulate and Limbic regions. Should they be functional they would be co-incident to MO with the other inputs.

Nearby outputs from both MOp and MOs are feedback to all SSp areas and to Vis-al and , and then numerous medium strength links to thalmic areas: MOp links to MD, PO, PF, RT, VPL, CM, VAL, VPMpc, and VM (listed in order of increasing distance; weights ~ 130 – 300), with a weaker (weight 30) link to CL; and MOs has feedback to Vis-am and Aud-p & -v, and again outputs to CL, MD, PO, RT, PF, VAL and VM. MOs also has feedback to associations areas: ACAd, ORB-vl & -l, AI-d and –v, PERI, ETC and TEa. MOp has strong feedback to AId (weights 350) and weaker structural links to ACAv, FRP, ORB-l and PTLp (weights 5, 50, 10, 20). Both MOp and MOs have longer range links to Striatum, Midbrain and most hind brain regions. Tracer experiments [60] have investigated the spatial organisation of L5 and L6 outputs from MOp and MOs, finding a segregation into a core of MOp projections to thalamic areas, enveloped in a shell of MOs projections.

Evolution of Module structure as Links are added

All of the results presented reflect the steady state modular structure of the mouse brain network, that is formed by all links present. Overall, shorter links are stronger and longer links are weaker (Figure 1). This is reflected in the sensory (Figure 4 and S5 - S7 Figures) and association (Figures 5, 6) circuits having a different character

when short or long links are included. Given a constant axonal signalling velocity, this is equivalent to a time evolution of links, e.g. following a sensory input event. Similar effects will determine the modular decomposition of the network when viewed through the lens of close vs. distant links. S9 Figure shown the modular decomposition of the mouse brain network calculated using the Infomap method at three stages of link evolution. Nodes are plotted now only in 2D for clarity. The first stage, shown at bottom, is formed by only short range links, of length d < 2 mm (1844 links). At this early stage there are three modules: the anterior module of 23 nodes joins the long term modules #2 (Somato-Motor) and #4 (Olf). The middle module of 74 nodes corresponds to #5 (Aud-Vis), while the posterior module of 116 nodes comprises the ultimate modules #1, 3, 6, 8 (medulla, pons, mid-brain, hypothalamus, hippocampus, cerebrum). At this early stage hierarchy is present: the anterior module separates Motor + Cingulate, Somatosensory, and Olfactory regions, amongst others, into 7 sub-modules. Similarly the middle module separates Auditory + temporal, Visual + Parietal, and Retrosplenial regions, while the posterior module separates into 7 sub-modules.

The intermediate stage of module formation, including the 12,145 links with d < 6 mm (about half the size of the brain) is shown as the mid-level in S9 Figure. Now the early stage modules are splitting into what is almost the final modular structure. This is driven by the inclusion of many more links between nodes. The vertical lines in the figure show the splitting pathways of the initial modules. Nodes are now colored by their ultimate module membership. The final stage, including all 14,103 links (ignoring weight < 1), is shown at the top. In summary, hierarchal modularity is only evident when only short range links are included. Many of those sub-modules become separate top-level modules when longer range links are included.

Signal flow along cortical gradients

Correlations amongst multi-modal cortical gradients [61] have been suggested as a brain organising principle, consistent with the concept of sensorimotor to transmodal spatial gradients [62]. Figure 7 shows the random walk forward transition probability, Pr(i:j) along successive steps of the SSp-bfd signalling pathway in the cortex, along with the MRI relaxation time ratio, T1w:T2w gradient along the same pathway. In each case there is a clear gradient, reminiscent of the spatial reference map previously found [61].

Figure 7. Cortical gradients along signal pathways. The node-to-node transition probability, Pr(i:j) plotted along the SSp-bfd sensory pathway in the cortex vs. the path distance (left axis and black filled circles; first neighbors only shown); and the MRI relaxation time ratio, T1w:T2w in cortex vs. the path distance (right axis and blue squares). The best linear fit to each set of points is shown.

Discussion

The Allen structural mouse connectome provides a rich data set to augment classical anatomical studies and from which to launch a more detailed investigation of brain networks and circuits. This can complement the many experimental probes that continue to provide details of specific pathways and circuits. The present analysis shows that some biologically relevant features can emerge from brain wide network analysis. Use of the full region-to-region connectivity data was justified (cf. Methods)

for most source regions. The connectivity data show a clear weight-distance fall off. This indicates that thresholds, to minimise false positives, may selectively penalise longer links, some of which may have functional significance. On average shorter links are stronger, while longer links are weaker (Figure 1). This partition shows up in the links from primary sensory regions to local cortical association areas, versus the longer range links between association areas and to the hind-brain state-keeping regions.

Simple network measures (Degree, nBC, eBC) alone do provide a sufficient guide to understanding overall network structure or important circuits. Such measures are based usually on graph shortest paths and so may be an incomplete guide to biologically important nodes or links. This is likely a symptom of the simplicity of the topological graph as a network model. Adding physically relevant features, such as spatial embedding, time evolution of links carrying fixed velocity signals, and including secondary paths for signal spread on the network, does provide a more informative model of the mouse brain network. However the participation coefficient highlights some nodes (e.g. CLA, ENTl, and possibly: CLI, PP, GPi, MGd, MOs) that turn out to mediate key linkages between network modules. A judicious selection of key nodes and links, informed by known biological functions, with a focus on sensory pathways and cortical association areas can reveal features of the mouse brain structural network consistent with evidence for biological functions. Tracing the primary sensory output paths over the network reveals selective roles of the various cortical association areas of the mouse brain shows local processing, and then progression on to the motor system.

Modular decomposition based on random walk (i.e. probability) flows over the network produces plausible division of network structures devoted to primary sensing, motor activity, information integration, and state maintenance (Figure 2). This is consistent with three views of the brain: as divided into the classical anatomical regions, as four inter-linked functional systems [57], and now as comprising 8 network modules. Three of these are aligned with primary sensory pathways: Olf (module #4), SSp+MO (#2), Aud+Vis (#5); two with the cortical association areas, separated into anterior (#7) and posterior (#5) locations; and the combined mid- and hind-brain regions (#1, #3, #6, #8). No hierarchy is detected at the resolution of linkage data currently available.

Sensory Pathways

The combined primary sensory pathways (Figures 4-6 and S5, S6 Figures) illustrate the direct, local and strong links to immediate targets, particularly in the motor and cortical association areas. The methods used herein show that the mouse isocortex can be seen in two parts, each with localised functions. The anterior senses (olfaction and somatosensory) align with the more anterior association areas: Insular, Limbic, Orbital and Cingulate. The more posterior senses (auditory, visual) interact more locally with the Temporal, Retrosplenial and Parietal association areas. Both anterior and posterior association areas have direct links to the motor regions. Secondary, in the sense of weaker and longer-range, links are between these two major regions and also including the Frontal Pole. Many cross modal structural links are present between the primary sensory regions.

The time progression of signals along sensory pathways reveals the roles of shorter vs. longer links (Figure 4). Close links are to the local cortical association areas and cross modal, while longer links provide anterior-posterior coordination and inputs to other brain regions. Figure 4b shows a number of nodes that appear as linkage hubs, some of which may have functional significance.
The successive network links from the primary sensory regions is consistent with observations of serial information flow from barrel field sensory to motor areas in a tactile decision task in mice [63].

The fabric of weaker structural links (weight < 1) is longer range and communicate with regions across the whole brain. On average the shortest path between any two nodes requires more steps (4.4 vs. 2) than over the full network with its large number of stronger, and generally shorter, links. The direct weak links are more to the hind-brain and the behavioural state system components (S6 Figure). Such weak structural links also have higher false positive rates, so only some may have functional significance. Cross-modal sensory links are common, as described above. These strong, close cross links between auditory and visuals pathways are consistent with observations of cross-modal attention and task choices in modulated audio-visual stimuli [64].

Cortical association areas

There is a clear anterior-posterior network localisation of cortical association areas, which are located close to relevant primary sensory regions. They tend to have direct strong links from nearby primary senses (Figures 5, 6) and outputs to other association areas and the motor regions. The frontal pole has very strong reciprocal links locally to Orbital, Insular and Motor regions; and is distinguished by having additional longer range connection (S7a Figure) to other brain regions. FRP also has numerous weaker and wide ranging links (S7b Figure).

Signal flow along cortical gradients

Correlations amongst multi-modal cortical gradients [61] have been suggested as a brain organising principle [61] that may provide an intrinsic coordinate system for human cortex [66]. The network description of signal pathways (Figures 4, S5, S6) is consistent with this view. Preliminary results here (Figure 7) show evident gradients along the mouse barrel field (SSp-bfd) pathway and justify further studies. Along that pathway short range near neighbor links have a higher forward transition probability compared to longer range links. There appears to be a signal flow gradient consistent with the T1w:T2w gradient has been previously suggested as a common spatial reference map [61].

Conclusion

Many layers of network features could be significant for brain function, as discussed in the Introduction. The question is which are necessary to reproduce, and even to predict, biologically relevant features. Random walks on the full structural linkage network produce modules consistent with anatomical and brain system functions [57, 58]. Biologically relevant hubs (e.g. CLA, ENTl) do appear as key linkage nodes identified by the participation coefficient and confirmed by the visualizations (Figures 3-6 and S5 Figure) ; other suggested hubs take more effort to identify as such. This highlights possible limitations of the network approach [65] at this time, and the need

to reformulate network models. Ultimately higher resolution will be also be required in both the connectivity data and the level of detail included in the network models.

Methods

Data

The original AIBS dataset [9] was used to generate the connectivity or adjacency matrix for the mesoscale mouse brain network. The experimental data was obtained using an anterograde viral tracer, labelled with a fluorescent probe, that was injected into a source region and allowed to spread along axonal projections to any linked target regions. Injection sites (source nodes) were located in the right hemisphere. Tracer was injected into 296 sites of the right hemisphere; some of which comprised several anatomical regions. Mutual connection strengths were measured to 296 ipsi-lateral and contra-lateral regions. Those injection sites may encompass several anatomical regions, so that some region-region connection strengths needed to be extracted in a model dependent manner [9, 18], which basically assumes a linear combination of contributions from each region, each of which is assumed to be uniform. Such assumption have been re-examined in detail for the cortical connections [18]. Of the 296 sites, some were omitted due to insufficient injection volume or not being well separable by the linear overlap model, resulting in 213 target regions that were determined to provide reliable results. Data were averaged over 400 adult male C57Bl/6J mice [9]. Here it is the ipsi-lateral data only that is examined.

The fluorescent detected in target anatomical regions provides a measure of the strength of the directed links between those source and target regions. The connection strength was defined in four ways [9, 16, 18], starting from the total volume of fluorescent signal detected in 100 mm voxels across a target region, normalised variously by the injection and/or target site volumes. Those volumes varied in size from 70 to 24,000 voxels, with the majority less than 5,000 voxels (i.e. 5 mm^3). Given the varying sizes of sources and targets, earlier analyses have calculated a "normalized connection density" as the fluorescent signal per unit volume of the target and per unit volume of the source [9, 16, 18]. However most network analysis typically deals with all weighted links between nodes, rather than density of links. Although some new methods allow for node weights, for example arising from city areas or brain region volumes, as well as link weights [67, 68], the significance of link density is not well developed in network models, so it is unclear how to apply this to brain data. Here we use the usual network model [6, 28] that incorporates varying node sizes and total link weights.

The original raw data is the normalized connection strength, originally termed w_{XY} [9], being the volume of fluorescent voxels detected in the target region arising from the volume of tracer injected in the source region, and was reported in Suppl. Table 3 of [9]. Whether this is the true network connection strength between the two regions is a question of volume sampling in the source region: a) did the injection volume sample all relevant axons projecting to the chosen target region? And b) did the viral injection infect a sufficient fraction of the source region to diffuse to all linked targets within the timescale of the experiments (up to 21 days [9])? For relatively larger regions, with fewer outward links and smaller injection volumes it is possible to miss

some efferent axons. That effect can be estimated by calculating a sampling metric for each region and experiment (injection volumes are listed in Supp. Table 2 of [9]). The metric $S_i = (Vol_i/k_i^{out})/\Delta V_i^{INJ}$, where Vol_i is the source region volume, k_i^{out} is the number of Out-links (or unweighted degree) from the source region (cf. S2b Figure) and ΔV_i^{INJ} is the mean injection volume. This calculation assumes the following: That the source region projects to k_i^{out} separate targets each of which, on average, accepts source axons from a fractional volume (Vol_i/k_i^{out}) of the source region; And that the injected volume ΔV_i^{INJ} does sample that fractional volume and so sense the relevant outgoing axon or fibre bundle. The use of multiple injections, as reported [9], increases the chance of correctly sampling relevant portions of the source region. S2b Figure shows that most regions have a large number of out links, with the most probable number being ~40-50, with mean 60. Reported injections had an average volume of 0.24 mm^3, in a range of 0.002 – 1.36 mm^3. While some regions are quite large (e.g. CP, MOB at 24 and 17 mm^3), the mean volume is 1.8 mm^3 while 56% are < 1 mm^3 and only 20 regions are > 5 mm^3. The latter contain likely candidates for under sampling. For $S_i < 1$ out links are likely to be well sampled since injected volumes, and their number, are large enough to span a sufficient volume of the source region. For $S_i > 1$ the injected volume is too small to sample all out links. The calculated metric was $S_i < 1$ for 96% of the 213 regions analysed, indicating that their out links are likely to be well sampled. For many of the smaller regions the injected volume spilled over into neighboring regions, necessitating a linear decomposition of signals to multiple separate target regions [9]. The calculated metric was $S_i > 1$ for nine cases, indicated those regions' Out-links were under sampled: FL, MDRNd, PAR, CP, MOB, Vispl, CA1 and PFL. Some (FL) were small with few out links, while others (CP, MOB) were large (24 & 17 mm^3) regions. All had 32 or fewer out links. The third largest region (PIR, 13 mm^3) had a marginal average score, $S_i = 1.18$, but the largest of those 7 injections (0.74 mm^3) yielded $S_i = 0.39$, possibly indicating good coverage. Of the 20 largest regions 5 were under sampled. By contrast CA3 is a relatively large region (5 mm^3) with few out links (32), so was flagged, but was well sampled (9 injections: 0.04 – 0.54 mm^3) so $S_i = 0.85$.

The extent of AAV infection of the source and all targets can be estimated with knowledge of the diffusion coefficient of AAV, measured as $D = 1.4\ \mu m/s^2$ [69]. For smaller injections of larger source regions time must be allowed for the viral tracer to diffuse across the region, to likely sources for distal targets. Typically the largest distance to travel would be half the size of a source region, which are in the range 0.2-1.5 mm. Order of magnitude estimates using the classical diffusion relation, $\langle r^2 \rangle = 6Dt$, indicates a worse case of order 10 days for the AAV tracer to diffuse over such distances. Subsequent transport along axonal pathways to target regions has also been modelled [70]. Overall the experimental timescale (up to 21 days [9]) appears to suffice for complete diffusion across source regions and along axons to targets. These tests indicate that the majority of measured normalized projection strengths are likely to reflect the true weight of source-target links, with the exceptions identified above. Thus use of the raw weights is justified, aside from the nine flagged cases where links weights are underestimated.

It is helpful for subsequent theoretical analysis to further normalise the measured values to some representative strength, so the link weights are hereafter scaled to a

unit value and are dimensionless. This is consistent with the common observation that many scientifically measured quantities have a typical size or scale [71]. Additionally well normalised quantities allow for more robust and efficient computation. As noted below the maximum and minimum measured values are possible outliers, so do not form a reliable basis for normalisation; and a layered data acceptance or rejection approach may be needed for concordance between structural and functional measurements. Thus some reliable, intermediate value needs to be chosen. Following the lower limit adopted in Figure 3 of [9] it is convenient to rescale the raw data by $a_0 = 10^{-3.5}$ (mm^3), which may then be taken as a unit link weight. The elements of the adjacency matrix, A are then well conditioned for matrix computations. Adjustments of this scale confirm that calculated network properties are unaffected by the specific choice. A model based argument can cast light on this scaling. Using the average density of 10^5 neuron/mm^3 in mouse cortex [72] suggests that about 3 neurons would fit in the cutoff volume. Thus the minimum link included in the adjacency matrix is plausibly close to one axon at this resolution, as noted by others [18]. The 14,192 links now included have strengths varying by nearly 10^5, as noted previously [9]. Each axon, on average, might have 100-1000 synapses [73, 74], so plausibly links of weight 10^{-2} should also be examined in subsequent sensitivity analysis. Using known average densities of neurons and synapses in mouse cortex [72] it can be estimated that, on average, those source and target regions may contain between 6.5k and 2.2m neurons, with most having around 500k neurons.

Data Thresholds

A simple plot of all 16,854 detected links is revealing. A log-linear plot of the original experimentally measured link strength vs. link distance (i.e. link length) is shown in S1 Figure, being the original quantitative connection strength (Suppl. Table 3 of [9]), that was described as the amount of segmented signal detected in the target region by infecting the source region [9]. S1 Figure highlights points lying beyond the main cluster of all other data, and that are likely to be outliers. The remaining cloud of data points shows more coherence and a clear trend, possibly linear, with link distance that is reminiscent of that found with diffusion MRI of human brain [43]. In that study the overall trend was quadratic, spanning 200 mm, however at the scale of the mouse brain (~12 mm) it was essentially linear.

It is widely recognised that the weakest measurements may constitute noise or be influenced by artefacts. Further some of the detected structural connections may not develop into functional links. Thus there is the question of choosing a threshold for the weakest links, and of establishing the correlation with functional links. The measured structural connectivity strengths span a large dynamic range with the weakest measurements being 10^{-16} below the strongest. Such a range might be commonplace in astrophysics but appears unusually large in the present context. The weakest ten measurements alone are 2-6 orders of magnitude below the main group of data and stand out as outliers in S1 Figure. The challenges of thresholding functional linkage measurements have been discussed in the context of generating binary, or unweighted, connectivity matrices [75]. Likewise the choice of threshold for the present structural data bears further study. The present structural linkage data, with its large range of weights, is amenable to examination by combining statistical data analysis methods with visualization. A standard approach is to plot and then de-trend the data, examine the distribution of residuals, and choose criteria for rejecting

outliers, most simply taken as data lying beyond three standard deviations from the (local) mean. Given the trend in the weight – distance log-linear plot it is clear that applying a simple threshold penalises longer range links, with proportionally more discarded. This can then inform the choice of threshold, which may need to be linkage distance dependent.

There is clearly a large variation in the raw connectivity data, suggesting possible sensitivity of the analysis to outliers in the data. Some care is required in applying the usual type of simple statistical tests, such as rejecting data more that three standard deviations from the mean, since that may eliminate potentially important links. Additional care needs to be taken to identify the correct sigma for the log-transformed data [76]. Beyond that, statistical measures of outlyingness [77], data depth and data concordance tests can inform such analysis. Similarly the physics and biology of the system can guide acceptance and rejection of outliers: important transitions in actual physical and social systems often exhibit data excursions of more than three standard deviations from the mean.

These original data [9] have been re-analysed and also compared to expert curation of a selected subset of original experiments [9, 18], to examine the effects of noise and co-injection thresholds [18]. Other studies have analysed the correspondence between structural links, measured by tracers, and connectivity measured by MRI diffusion tractography [45]. And others [55, 46] focussed on links in the mouse isocortex, or the visual cortex [78]. Statistical analysis of the tradeoffs between True- and False-Positives rates, represented in so-called Receiver Operating Characteristic (ROC) curves [79], provides a measure of the correspondence between different connectivity measurements. The MRI tractography comparison produced a true-positive rate of 61% and a false-positive rate of 26% [45], suggesting a quantifiable approach to thresholding. Using a family of ROC curves at varying thresholds indicated that selection of the top 40% of structural links improved the correlation between structural and functional (rs-fcMRI) measurements [46]. The correspondence between the original raw measurements and expert curation (cf. Extended Data Figure 7 of [9]), of a random sample of 20 images, indicated a False Positive rate of 14.5% at the threshold a_0 ($10^{-3.5}$ mm^3), mostly due to image artefacts or low signal levels, possibly confounded with noise. Thus the present study focuses on the top 40%, by weight, of structural links by applying a link weight threshold, at weight 78 using the normalisation described above. The sensitivity of results to threshold choice is investigated and the weak links are studies separately.

The present analysis also required the distance matrix which records link lengths between nodes. Geometric distances between nodes (anatomical regions) were taken from the coordinates available online with the Allen Atlas [12, 13]: the Waxholm space delineation 2012 (V2) for the C57BL/6 mouse was used, since this was then contemporary with the connectome experiments and is still used in various AIBS online products. A later, higher resolution, edition, the Allen Mouse Brain Common Coordinate Framework version 3, was used to check selected results, noting the different coordinate origin. In the present application only distances between nodes were required. The centroid (median values of x, y, z) of each region was used as a representative node coordinate; typically this would be close to the centre of mass, except for regions of unusual shape. Available 3D volumes of Nissl-stain sections and labels at voxel level, along with NIFTI tools in Matlab [80] enabled comparison

between the three sources. Typically differences up to 0.2mm were encountered, with larger, extended anatomical regions (e.g. MO) being more difficult to characterise by a single coordinate. Here geometric effects are limited to the influence of link length and strength on network features – rather than geometric constraints, such as a finite brain volume constrained by a rigid skull.

Network analysis

The network analysis methods were described previously and tested on the mouse retina connectivity data [11] and follow standard practice [1, 5-7, 28]. The nodes of network are the 213 anatomical regions corresponding to the selected experimental source (injection sites, or combinations thereof) and target sites [9]. The resultant array of source-target link strengths forms the adjacency matrix [5, 6, 28] for subsequent analysis. This matrix is directed and weighted, and scaled as described above. Self-links, returning to the injection site, are omitted in the present study. Thus the adjacency matrix has zero entries along its diagonal. Subsequent analysis proceeds from the adjacency matrix, whose entries, A(i,j) encode the weight and direction of links between nodes i and j, chosen from the 213 anatomical regions. The matrix is not symmetric since the network links are directed. The diagonal elements are zero since self-loops, present in the original data, are ignored in the present analysis. Thus there are (n-1)(n-2) = 44,732 possible directed links between the 213 chosen anatomical regions. The adjacency matrix was thresholded, normalised and filtered as described above (cf. S1 Figure).

Many of the usual network measures have been applied to brain data [1, 5, 50], and indeed to the mouse data [9, 16], to rank the importance of nodes and links. These can reflect different features of the underlying network structure [81, 82] and probe different types of process occurring on the network. The simplest measure, node degree, reflects local structure – that is nearest neighbour links, or paths of length one step. Degree also yields the long-time probability of visits by a random walker to the node [29, 33]. For directed links in-degree and out-degree are distinguished. Node strength, or weighted degree, generalises the concept of degree to a weighted network.

Centrality measures probe more global aspects of the network such as how non-adjacent nodes communicate and can identify which are the "central" nodes in the network. Degree is the simplest such measure. Others are the node betweenness centrality (nBC) [83] and edge BC (eBC) [6, 28]. The commonly used centrality measures are based on graph or network concepts such as shortest graph paths or geodesics. Those count the number of intervening topological steps between nodes. This is distinct from the geometric path length, which reflect the distance travelled between nodes along links in physical space. From graph theory the Dijkstra algorithm [83] facilitates computation of the shortest paths and is embodied in many of the standard codes [84]. Note that the un-weighted links are used for that calculation. The restrictions described can be problematic, so care is needed in applying the methods and interpreting the results. For instance, nodes with many low-weight links may be emphasised over those with few high weight links. The standard methods do not take into account the spatial locations of neurons and the spatial embedding of the network structure; nor do they allow for routing of signal flows via indirect pathways as well as via shortest paths. They are appropriate to phenomena that embody targeted flow such as package delivery via a specified route in a transportation network, or disembodied interactions such as in a social network, rather

than spreading phenomena on networks, such as diffusive flows or random walks. In brains where signals or pulse trains, that may encode information transmitted over axons and synapses, can spread by both direct paths and also via secondary links or more circuitous paths. This can have both deterministic and stochastic elements, so a random walk centrality measure (rwC), developed in other contexts [33], may be relevant. Node degree and the various node centrality measures (nBC, eBC, rwBC) were calculated by standard methods and toolboxes using available Matlab codes [84].

Modular decomposition

Many methods have been applied to the analysis of nervous system and brain connectivity matrices [5, 24, 32]. These identify groupings of locally well-connected nodes that are more frequently or more strongly connected within modules than between them. A modularity metric often is used to compare different partitions, specifically Newman's Modularity Q [52, 53] which compares a found partition to a null model (random, configuration model). In the present study three representative methods are used to detect modules in the mouse structural connectome.

The InfoMap algorithm uses information theoretic concepts (Hoffman code length) that are equivalent to following random walks on the network [48]. Such are well suited to studying spreading phenomena on networks [81]. As implemented it uses a first order, i.e. one step, markov process. The infomap method also has been extended to two step processes, which can reveal additional modular features [85]. Such methods align well with the essential feature of a brain network, to host signal flows on the network of neurons and synapses. Modules found by this method are essentially groups of nodes in which a random walker spends a larger fraction of time. An efficient C++ code and online apps are available [86]. This method has been shown to perform well on a range of test cases [48, 49], and has been applied successfully to the mouse retina connectivity data [11].

Other methods commonly applied to neuroscience networks include the Louvain method [54], which iteratively agglomerates neighbouring nodes into clusters, that form super nodes that then are aggregated, while monitoring the modularity metric. Both Matlab and C++ codes are available [84]. The Louvain and InfoMap algorithms generally produce similar results and have proved useful for biological systems, including brain networks. Both methods can uncover hierarchical modular structure. Classical methods in network science also use spectral partitions which cluster leading eigenvectors of the adjacency matrix or its associated Laplacians [52, 53]. The number of modules sought has to be specified in advance, and may be limited to 2 for some methods. These and other traditional clustering algorithms, such as agglomerative or divisive methods [54], do not always generalise to weighted, directed (in non-binary) networks, or use metrics calculated from shortest graph paths on the network. It is becoming increasingly evident that such methods may be less appropriate for brain networks that are spatially embedded, time dependent, weighted and directed. Herein the InfoMap method was used primarily, and compared with the other methods described.

Temporal Networks

Time dependent phenomena can unfold on and spread over the fixed network [35-37]. The signalling is not instantaneous; rather signals (both individual action potentials

and pulse trains) travel along the network of axons at a fixed velocity. Thus both the network structure and the biophysics of signalling on the network determine where and when signals arrive at waypoints and putative targets. As was shown for light signalling by the special theory of relativity in 1905, so too for signalling on a network of nerves there will be an expanding space-time cone of reachable targets [38]. Signal velocity may vary between axons since it depends on axon diameter and degree of myelination [87]. Measurements of signal delays in a mouse thalamus-M1-ALM (pre-motor) circuit [88] indicate an axon conduction velocity of order ~ 1m/s, or equivalently 1 mm/millisec (mm/msec). This ignores variability with axon diameters and myelination. Raman scattering microscopy of mouse brain indicates ~10% region to region variation of myelin density [86]; the images indicate fairly constant myelin thickness along fibre tracts. Absent further information it is assumed here that all signal velocities over links are constant. The analysis also needs estimates of synaptic delay for multi-hop signal paths, here taken as 2 ms [89], which can be taken as equivalent to a 2 mm additional path length. Thus link length (mm) can be taken as a proxy for signal delay over that link (in msec).

Analysis and visualization of temporal, or time evolving, links involves choosing a specified source node[s], finding the list of target nodes, with in- or out-links, then re-ordering these by increasing link lengths, and drawing them in distance, or equivalently time, sequence. For links longer than ~5-6 mm (about half the brain size for the mouse) it is possible for 2-step links to be simultaneously active in the distance (time) window and thus warrant examination. The mid node was already directly linked to the source node, so credibly signals could continue on to/from a relevant target/source node. For those second links the synaptic delay needs to be included to correctly describe signal traversal across two links. A representative synaptic delay of 2 msec, measured in mouse neocortical pyramidal neurons [88], and signalling speed (i.e. axon velocity) of 1 mm/ms, adds an equivalent path length of 2 mm for the purposes of visualizating 2-step links.

Schematic coordinates and 3D visualization

Plots of even medium sized networks with many links quickly become too dense to be intelligible. While many such visualizations are presented as network layouts in 2D, most can be generalised to 3D graphics, the latter requiring zooming, panning and rotations to identify and follow linkages. The brain is intrinsically a 3D structure, where spatial proximity is important for signalling so we need methods that enable its visualization in 3D. Neuroscientists often use 2D projections, sometimes in orthogonal pairs, to represent the anatomical layout brain regions.

A standard challenge in information visualization is choosing a simplified, schematic representation of a complex system, such as a network, that captures the essential features of the system and aids insight by presenting a 2D or 3D image that promotes intuition [90]. In so doing it is essential not to misrepresent structural or other important information. A long standing approach to presenting complex, spatially embedded networks is a schematic layout. Beck's 1932 schematic layout of the London underground rail network [91] is the classic example, variants of which have been widely adopted in major cities. It enables commuters to find their route in the complex network of rail links at a glance. Rather than faithfully tracing the rail links on the city map, a schematic map is developed. This simplifies major geographic features, such as the Thames river, to be nearly linear. The nodes (stations) are laid

out on an almost rectangular grid. Linkages are generally straight lines drawn at a few regular angles. Together these steps reduce the visual congestion. In so doing it is important to keep a balance and not omit important structure. Overall the graphic captures the essential features of the network and omits myriad geographic details.

Noting the visual complexity of S4 Figure, it may be beneficial to test a simplified schematic layout of the mouse brain network. To that end, a set of schematic coordinates was developed, in which the original 213 anatomical regions, located at the Allen Atlas coordinates, were condensed onto 55 locations which each aggregated related and nearby regions (eg. combine ORBl, ORBm, ORBvl together; and ACAv, ACAd; and AUDd, AUDp, AUDv; and GU, VISC; and RSPd, RSPv, RSPagl; and ECTm TEa; for the mid- and hind-brain regions nodes were gathered into 2-4 groups along the anterior-posterior axis); the 35 sub regions of the Thalamus were divided into 6 groups, and the Isocortex into 14 groups. Typically these are closer to each other than the region's size (cf. voxel count in S2 Data). Vis and SSp are a special cases with each encompassing several separate sensory pathways, so their nodes were assembled into a small square grid rather than a single point. A guide was provided also by the essentially cylindrical symmetry of the anatomical regions in the Allen Atlas: with a clear anterior-posterior progression, and also an approximately radial separation of medial vs. lateral regions in a single hemisphere. Regions were typically divided into 2-5 sub-regions; however the isocortex, with more identified functional regions, was sub-divided into 22 sub-regions. The chosen coordinates are listed in S3 Data, where they are listed by region and in order of anterior-posterior location, and illustrated in S10 Figure. A benefit of this approach is that related links, often between nearby related nodes, become bundled into a few pathways, thereby enabling navigation of the 3D visualizations. They can be un-bundled, as required, to uncover local linkage details. Now all nodes and all links can be plotted in a graph with some prospect of navigating the link pathways. Subsequent figures place nodes at these schematic coordinates. Similarly, the 3D convex hull surfaces (Figure 2) are used to represent brain regions is a schematic approximation. Not being space filling it causes an "exploded view" in 3D of brain regions and reduces crowding in the images. Surface colours match those presented in the Allen Brain Atlas sagittal slice images [92]. All figures were produced in Matlab, with all codes available [93].

Acknowledgments
The author thanks P Robinson and P Gong for support and valuable discussions, and acknowledges B Fulcher for valuable suggestions.

Author Contributions
Conceptualization: BAP. Formal analysis: BAP. Investigation: BAP. Software, visualization: BAP. Writing – original, review: BAP.

References
1. Bullmore E, Sporns O. Complex brain networks: graph theoretical analysis of structural and functional systems. Nature Rev. Neurosci. 2009; 10: 186-198. doi:10.1038/nrn2575.

2. Denk W, Briggman KL, Helmstaedter M. Structural neurobiology: missing link to a mechanistic understanding of neural computation. Nature Rev. Neurosci. 2012; 13: 351-358.

3. Fornito A, Zalesky A, Breakspear M. Graph analysis of the human connectome: Promise, progress, and pitfalls. NeuroImage. 2013; 80: 426–444. rights reserved. http://dx.doi.org/10.1016/j.neuroimage.2013.04.087.

4. Bassett DS, Zurn P, Gold JI. On the nature and use of models in network neuroscience. Nature Rev. Neurosci. 2018; 19. 566-578. https://doi.org/10.1038/s41583-018-0038-8.

5. Sporns O. (2011) Networks of the Brain. MIT Press.

6. Newman MEJ. The Structure and Function of Complex Networks. SIAM Review. 2003; 45(2): 167–256. www.siam.org/journals/sirev/45-2/42480.html.

7. Fortunato S. Community detection in graphs. Phys. Rep. 2009; 486(3): 75–174.

8. Scanziani M, Michael Häusser M. Electrophysiology in the age of light. Nature. 2009; 461: 930-939. doi:10.1038/nature08540.

9. Oh SW, Harris JA, Ng L, Winslow B, Cain N, et al. A mesoscale connectome of the mouse brain. Nature. 2014; 508: 207-214. doi:10.1038/nature13186.

10. Helmstaedter M, Briggman KL, Turaga SC, Jain V, Seung HS, Denk W. Connectomic reconstruction of the inner plexiform layer in the mouse retina. Nature. 2013; 500: 168–174. doi:10.1038/nature12346. PMID: 23925239.

11. Pailthorpe BA. Network Analysis of Mouse Retina Connectivity Data. PlosOne. 2016; 11(7): e0158626. doi:10.1371/journal.pone.0158626.

12. Bakker R, Tiesinga P, Kotter R. The Scalable Brain Atlas. Neuroinformatics. 2015; 13: 353–366 DOI 10.1007/s12021-014-9258-x.

13. Allen Brain Atlas, hosted at http://scalablebrainatlas.incf.org.

14. Harris JD, Mihalas S, Hirokawa KE, Whitesell JD, Knox J, Bernard A. et al. The organization of intracortical connections by layer and cell class in the mouse brain. bioRxiv 2018; Preprint. http://dx.doi.org/10.1101/292961.

15. Robinson PA. Physical brain connectomics. Phys. Rev. E 2019; 99: 012421.

16. Rubinov M, Ypma RJF, Watson C, Bullmore ET. Wiring cost and topological participation of the mouse brain connectome. PNAS. 2015; 112(32):10032–10037. doi: 10.1073/pnas.1420315112 PMID: 2621696

17. Fulcher BD, Fornito A. A transcriptional signature of hub connectivity in the mouse connectome. PNAS. 2016; 113(5): 1435-1440. doi.org/10.1073/pnas.1513302113.

18. Ypma RJF, Bullmore ET. Statistical Analysis of Tract-Tracing Experiments Demonstrates a Dense, Complex Cortical Network in the Mouse. PLoS Comput. Biol. 2016; 12(9): e1005104. doi:10.1371/journal.pcbi.1005104.

19. Betzela FR, Bassett DS. Multi-scale brain networks. Neuroimage. 2017; 160, 15: 73-83. https://doi.org/10.1016/j.neuroimage.2016.11.006.

20. Gozak M, Markovic R, Jurij Dolens J, Rupnik MS, Marhl M. et al. Network science of biological systems at different scales: A review. Physics of Life Reviews. 2018; 24: 118–135. https://doi.org/10.1016/j.plrev.2017.11.003.

21. Liu W, Suzumura T, Ji H, Hu G. Finding overlapping communities in multilayer networks. PloS One 2018; 13(4): e0188747. https://doi.org/10.1371/journal.pone.0188747

22. Henderson JA, Robinson PA. Geometric effects on complex network structure in the cortex. Physical Review Letters. 2011; 107: 018102. https://doi.org/10.1103/PhysRevLett.107.018102.

23. Roberts JA, Perry A, Lord AR, Roberts G, Mitchell PB, Smith RE. Calamante F, Breakspear M. The contribution of geometry to the human connectome. NeuroImage. 2016; 124 A: 379-393. http://dx.doi.org/10.1016/j.neuroimage.2015.09.009

24. Stiso J, Bassett, DS. Spatial Embedding Imposes Constraints on Neuronal Network Architectures. Trends Cog. Sci. 2018; 22(12): 1127-1142. https://doi.org/10.1016/j.tics.2018.09.007.

25. Chklovskii DB, Schikorski T, Stevens CF. Wiring Optimization in Cortical Circuits. Neuron, 2002; 34: 341–347. https://doi.org/10.1016/S0896-6273(02)00679-7

26. Bullmore, E, Sporns O. The economy of brain network organization. Nature Rev. Neurosci. 2012; 13: 336-349. doi:10.1038/nrn3214.

27. Barthelemy M. Spatial networks. Physics Reports. 2011; 499: 1–101.

28. Albert R, Barabasi, A-L. Statistical mechanics of complex networks. Rev. Mod. Phys. 2002; 74: 47-97.

29. Masuda N, Porter MA, Lambiotte R. Random walks and diffusion on networks. Phys. Reports. 2017; 716-717: 1-58. dx.doi.org/10.1016/j.physrep.2017.07.007.

30. Fortunato, S. Community detection in graphs. Phys. Rep. 2009; 486(3): 75–174.

31. Simon H. The architecture of complexity. Proc. Am. Philos. Soc. 1962; 106: 467–482.

32. Meunier D. Lambiotte R. Bullmore ET. Modular and hierarchically modular organization of brain networks. Front. Neurosci. 2010. 4, 1-11. doi:10.3389/fnins.2010.00200

33. Newman ME, A measure of betweenness centrality based on random walks. Social Networks. 2005; 27(1); 39-54. https://doi.org/10.1016/j.socnet.2004.11.009.

34. Henderson JA, Robinson PA. Using Geometry to Uncover Relationships Between Isotropy, Homogeneity, and Modularity in Cortical Connectivity. Brain Connectivity. 2013; 3(4): 423-437. DOI: 10.1089/brain.2013.0151

35. Kovanen L, Karsai M, Kaski K, Kertesz J, Saramaki J. Temporal motifs in time-dependent networks. J. Statistical Mechanics: Theory and Experiment. 2011; 2011: P11005. doi:10.1088/1742-5468/2011/11/P11005. http://iopscience.iop.org/1742-5468/2011/11/P11005.

36. Holme P. Saramarki J. Temporal Networks. Physics Reports. 2012; 519(3): 97-125.

37. Holme P. Modern temporal network theory: a colloquium. Eur. Physics Journal, B. 2015; 88: 234-264.

38. Halliday D, Resnick R, Waller J. Fundamentals of Physics Extended. Wiley, 5th Ed. 1997; Ch 38.

39. Stein BE, Stanford TR. Multisensory integration: current issues from the perspective of the single neuron. Nat. Rev. Neurosci. 2008; 9: 255-266. doi:10.1038/nrn2331.

40. Valencia M. J. Martinerie J. Dupont S. Chavez M. Dynamic small-world behavior in functional brain networks unveiled by an event-related networks approach. Physical Review E. 2008; 77: 050905-1-3. DOI: 10.1103/PhysRevE.77.050905.

41. Buzaki G, Llinas, R. Space and Time in the Brain. Science. 2017; 358: 482-485. DOI: 10.1126/science.aan8869.

42. Knox JE, Harris KD, Graddis N, Whitesell JD, Harris JA. et al. High resolution data-driven model of the mouse connectome. Network Neuroscience. 2019; 3(1): 217-236. doi:10.1162/netn_a_00066.

43. Roberts JA. Perry A. Lord AR. Roberts G.Mitchell PB. Smith RE. Calamante F. Breakspear M. The contribution of geometry to the human connectome. NeuroImage. 2016; 124A: 379-393. http://dx.doi.org/10.1016/j.neuroimage.2015.09.009.
44. Choi H. Mihalas S. Synchonization dependent on spatial structures of a mesoscopic whole-brain network. PLoS Comp Bio. 2019; 15(4): e1006978. https/doi.org/10.1371/journal.pcbi.1006978.

45. Calabrese E, Badea A, Cofer G, Qi Y, Johnson GA. A Diffusion MRI Tractography Connectome of the Mouse Brain and Comparison with Neuronal Tracer Data. Cerebral Cortex. 2015; 25(11): 1-10.

46. Stafford JM. et. al. Large-scale topology and the default mode network in the mouse connectome. PNAS. 2014; 111(52): 18745–18750. www.pnas.org/cgi/doi/10.1073/pnas.1404346111.

47. Grandjean J. Zerbi XV. Balsters JH. Wenderoth N. Rudin M. Structural Basis of Large-Scale Functional Connectivity in the Mouse. J. Neuroscience. 2017; 37(34): 8092– 8101. DOI:10.1523/JNEUROSCI.0438-17.2017.

48. Rosval M, Bergstrom CT. Maps of random walks on complex networks reveal community structure. PNAS: 2008; 105(4): 1118–1123. doi:10.1073/pnas.0706851105 PMID: 18216267

49. Rosval M, Bergstrom CT. An information-theoretic framework for resolving community structure in complex networks. PNAS: 2007; 104(18): 7327–7331. PMID: 17452639

50. Guimera R, Nunes-Amaral LA. Functional cartography of complex metabolic networks. Nature. 2005. 433. 895-900. doi:10.1038/nature03288.

51. Sporns O, Honey CJ, Kotter R. Identification and Classification of Hubs in Brain Networks. Plos One. 2007; 2(10): e1049. doi:10.1371/journal.pone.0001049.

52. Newman MEJ, Girvan M. Finding and evaluating community structure in networks. Phys. Rev. E: 2004; 69: 026113.

53. Newman MEJ. Finding community structure in networks using the eigenvectors of matrices. Phys. Rev. E: 2006; 74: 036104.

54. Newman MEJ. Fast algorithm for detecting community structure in networks. Phys. Rev. E. 2004; 69 (6), 066133.

55. Blondel VD, Guillaume J-L, Lambiotte R, Lefebvre E. Fast unfolding of communities in large networks. J. Stat. Mech. Theory and Expt. 2008; 10: P10008.

56. Zing B. Hintiryan H. Gou L. Song MY. Bay M. Bienkowski MS. Foster MN. Yamashita S. Bowman I. Arthur W. Toga AW. Dong H-W. Neural Networks of the Mouse Neocortex. Cell 2014. 156. 1096-1111. http://dx.doi.org/10.1016/j.cell.2014.02.023.

57. Swanson L. Brain Architecture. Oxford University Press. 2012.

58. Kandel ER, Schwartz JH, Jessell TM. Principles of Neuroscience. Fourth Ed. McGraw-Hill. 2000.

59. Onnela J-P, Saramaki J, Hyvonen J, Szabo G, Lazer D, et al. Structure and tie strengths in mobile ommunication networks PNAS. 2007; 104(18): 7332–7336. www.pnas.org/cgi/doi/10.1073/pnas.0610245104.

60. Jeong M, Kim Y, Kim J, Ferrante DD, Mitra PP, et al. Comparative three-dimensional connectome map of motor cortical projections in the mouse brain. Sci. Reports. 2016; 6:20072, 1-14. DOI: 10.1038/srep20072.

61. Fulcher BD, Murray JD, Zerbi V, Wang X-J. Multimodal gradients across mouse cortex. PNAS. 2019; 116(10): 4689–4695. www.pnas.org/cgi/doi/10.1073/pnas.1814144116.

62. Marguiles DS, Ghosh SS, Goulas A, Falkiewicz M, Huntenburg JM. et al. Situating the default-mode network along a principal gradient of macroscale cortical organization. PNAS 2016; 113(44): 12574–12579. www.pnas.org/cgi/doi/10.1073/pnas.1608282113.

63. Guo ZV, Li N, Huber D, Ophir E, Gutnisky D, et al. Flow of Cortical Activity Underlying a Tactile Decision in Mice. Neuron. 2014; 81: 179-194. http://dx.doi.org/10.1016/j.neuron.2013.10.020.

64. Wilson AM, Beck JM, Glickfield LL. Separable codes for read-out of mouse primary visual cortex across attentional states. biorxiv Preprint. 2019; dx.doi.org/10.1101/731398.

65. Papo D. Zanin M. Pineda-Pardo JA. Boccaletti S. Buldu JM. Functional brain networks: great expectations, hard times and the big leap forward. Phil. Trans. Roy. Soc. B. 2016. 369. 20130525. http://dx.doi.org/10.1098/rstb.2013.0525

66. Huntenburg JM, Bazin P-L, Margulies DS. Large-Scale Gradients in Human Cortical Organization. Trends Cog. Sci. 2018; 22(1): 21- 31. https://doi.org/10.1016/j.tics.2017.11.002.

67. Heitzig J, Donges JF, Zou Y, Marwan N, Kurths J. Node-weighted measures for complex networks with spatially embedded, sampled, or differently sized nodes. Eur. Phys. J. 2012; 85: 38. https://doi.org/10.1140/epjb/e2011-20678-7.

68. Weidermann M, Donges JF, Heitzig J, Kurths J. Node-weighted interacting network measures improve the representation of real-world complex systems. Eur. Phys. Lett. 2013; 102(2): 280078. https://doi.org/10.1209/0295-5075/102/28007.

69. Seisenberger G, Reid MU, Endre T, Bunning, H, Hallek M, et al. Real-time single-molecule imaging of the infection pathway of the Adeno-Asociated Virus. Science. 2001; 294(5548): 1929-1932. DOI:10.1126/science.1064103.

70. Dinh A-T, Theofanouse T, Mitragoti S. A model of intracellular trafficing of Adenoviral vectors. Biophys. J. 2005. 89(3): 1574-1588. https://doi .org/10.1529/biophysj.105.059477.

71. Newman MEJ. Power laws, Pareto distributions and Zipf's law. Contemp. Phys. 2005; 46(5): 323-351. DOI: 10.1080/00107510500052444.

72. Harris KD, Shepherd GMG. The neocortical circuit: themes and variations. Nature Rev. Neurosci. 2015; 18(2): 170-181. doi:10.1038/nn.3917.

73. Le Duigou C. Jean Simonnet J. Teleñczuk MT. Fricker D. Miles R. Recurrent synapses and circuits in the CA3 region of the hippocampus: an associative network. Front. Cell. Neurosci. 2014. 7. 262-x. https://doi.org/10.3389/fncel.2013.00262.

74. Kasthuri N, Hayworth KJ, Berger DJ, Schalek RL, Conchell JA, et al. Saturated Reconstruction of a Volume of Neocortex. Cell. 2015; 162: 648-661. http://dx.doi.org/10.1016/j.cell.2015.06.054.

75. Garrison KA, Scheinost D, Finn ES, Shen X, Constable RT. The (in)stability of functional brain network measures across thresholds. 2015. Neuroimage. 118. 651–661. doi: 10.1016/j.neuroimage.2015.05.046.

75. Press WH, Teukolsky SA, Vetterling WT, Flannery BP. Numerical Recipes, Third Ed. Cambridge University Press. 2007.

77. Barnett V, Lewis T. Outliers in statistical data. Wiley, 1994.

78. Wang Q. Sporns O. Burkhalter A. Network Analysis of Corticocortical Connections Reveals Ventral and Dorsal Processing Streams in Mouse Visual Cortex. J Neuroscience. 2012. 32(13). 4386–4399.

79. Hanley JA, McNeil BJ. The meaning and use of the area under the Receiver Operating Characteristic (ROC) curve. Radiology. 1982; 143(1): 29-36.

80. NIFTI tools available at http://mathworks.com/matlabcentral/fileexchange/8797-tools-for-nifti-and-analyze-image.

81. Borgatti SP. Centrality and network flow. Social Networks. 2005; 27: 55-71.

82. Latora V, Marchiori M. A measure of centrality based on the network efficiency. New J. Phys. 9, 188. doi:10.1088/1367-2630/9/6/188.

83. Brandes U. A Faster Algorithm for Betweenness Centrality. J Math. Sociology. 2001; 2: 163-177.

84. Network code libraries:
BCT. Rubinov M, Sporns O. Complex network measures of brain connectivity: uses and interpretations. Neuroimage. 2010; 52: 1059–1069. Available at: https://sites.google.com/site/bctnet/
GAIMC. Gleich D. 2009; Available at: www.mathworks.com/matlabcentral/fileexchange/24134-gaimc---graph-algorithmsin-matlab-code.
BGL 2008; http://www.mathworks.com/matlabcentral/fileexchange/10922-matlabbgl.

85. Schaub MT, Rosval M, Lambiotte R. The many facets of community detection in complex networks. Applied Network Science. 2017; 2: 4. DOI 10.1007/s41109-017-0023-6.

86. Rosval M. Infomap codes and tutorial, available at: www.mapequation.org.

87. Fu Y, Huff B, Wang H-W, Wang H, Cheng J-X. Ex vivo and in-vivo imaging of myelin fibres in mouse brain by coherent ant-stokes Raman scattering microscopy. Opt. Express. 2008; 16(24): 19396-19409. https://doi.org/10.1364/OE.16.019396.

88. Guo ZV, Inagaki HK, Kayvon Daie K, Druckmann S, Gerfen CR, Svoboda K. Maintenance of persistent activity in a frontal thalamocortical loop. Nature. 2017; 545: 181-186. doi:10.1038/nature22324.

89. Izquierdo-Serra M, Hirtz JJ, Shababo B, Yuste R. Two-Photon Optogenetic Mapping of Excitatory Synaptic Connectivity and Strength. iScience. 2018; 8: 15-28. https://doi.org/10.1016/j.isci.2018.09.008.

90. Tufte ER. The visual display of quantitative information. Graphics Press, Cheshire, Ct. 1983.

91. Whitfield P. London: A Life in Maps. 2007; The British Library, London.

92. Allen mouse brain atlas (Saggital images) http://mouse.brain-map.org/statoc/atlas.

93. Matlab codes used herein available at: gihub….

Supporting Information

S1 Data. Weighted, directed adjacency matrix for the 213-node mesoscale ipsi-lateral mouse brain connectome (160 KB CSV text file).

S2 Data. Details of all 213 nodes along with network measures (93 KB XLS text file).

S3 Data. Schematic coordinates of the 213 nodes (62 KB XLS text file).

S1 Figure. All experimentally detected link strengths plotted as $\log_{10}$(strength) vs. distance. The strength used is the quantitative projection strength reported in the original Supplm. Table 3 of [9]. The plot highlights the 10 lowest outliers (red).

S2 Figure. a. Distribution of weighted Degree-In and –Out for all 213 nodes. **b**. Distribution of un-weighted Degree-In and –Out, i.e. the number of links in and out of each node.

S3 Figure a. Distribution of graph path lengths (i.e. number of link between any two nodes) and **b**. Distribution of link distances in geometric space.

S4 Figure. All nodes (anatomical regions) plotted in Allen coordinates and their Out-links. Nodes are colored by their module membership (cf. Table 1 and S2 Data), and links by the module membership of the target nodes.

S5 Figure. **a**. Strong out links (top 40%) from primary senses (listed in text; cf. Figure 4) for medium length links ($5 < d < 6.5$ mm); and **b**. for longer ($6.5 < d < 10$ mm) links. Shorter links ($d < 5$ mm; cf. Figure 4a) are omitted for clarity. Visually evident hubs in mostly ventral regions include, from right to left: DP, ACB, CP, EPd and (posterior) PERI, as described in the main text.

S6 Figure. Weak Out-links (weight < 1) from primary sensory areas (cf. Figure 4) plotted in schematic coordinates, for link lengths: **a**. $d < 6.5$mm; and **b**. $d < 10$mm. Nodes are colored by their module membership, and links by the module membership of the target node. Heavier lines are caused by overwriting multiple links along the same paths.

S7 Figure. **a**. Strong (top 40%) In- and Out-links with Frontal Pole. Stronger links (weight >1 and > 5k) are highlighted by thicker lines. **b**. Remaining weak In- and Out-links with Frontal Pole. Nodes are colored by their module membership, and links by the module membership of the target node. Note a number of 2-step links are possible.

S8 Figure. Strong (top 40%) In-links to Motor areas (MOp, on the left, and MOs, on the right – both highlighted as larger circles), plotted in schematic coordinates. Stronger links (weight >1 and > 5k) are highlighted by thicker lines. Links are colored according to their source module.

S9 Figure. Evolution of modular structure in the mouse connectome. Nodes are plotted in schematic coordinates condensed into a 2D plane. At each stage the Infomap method included only links up to a certain length. The initial structure of 3 larger modules, formed by shorter range (< 2 mm) links is shown at bottom; intermediate structure (links < 6 mm) at middle, where nodes are now colored by the final module membership; and final structure with 8 modules, formed by all links, shown at top. Vertical lines show splitting of early modules into their ultimate components.

S10 Figure. All 213 nodes plotted at the 45 schematic coordinates (listed in S3 data). The brain regions are represented by the encompassing convex hull (Fig 2), with other features as in S4 Figure. **a**. 3D perspective view from above the right front; **b**. view from left rear.

S1 Table. Top 20 nodes in order of decreasing probability flow calculated by the Infomap method [49], with other network measures listed. (59 KB PDF text file).

S2 Table. Likely hub nodes have high participation coefficient, P and weighted in-Degree or Out-Degree (30 KB PDF text file).

S3 Table. Comparison of Infomap modules with those found by the Louvain and the Newman spectral bisection methods. Infomap modules are list in approximately Anterior-Posterior and sensory-motor-midbrain-hindbrain order (24 KB PDF text file).

S1 Table. Flow, top 20

ID	Acrn	Region	Flow	Deg In, wt	Deg Out, wt	Deg In, unwt	Deg Out, unwt	rwC	nBC	Module
36	CP	Striatum	0.0588	453075	2360	87	22	0.0431	78	2
100	MRN	Midbrain	0.0486	182960	5647	88	77	0.0495	9	1
117	PAG	Midbrain	0.0330	164629	6368	98	101	0.0339	0	1
161	SCm	Midbrain	0.0314	215384	7160	78	74	0.0294	271	1
75	LHA	Hypothalamus	0.0288	149643	10634	110	114	0.0265	371	3
139	PRNc	Pons	0.0247	44790	6850	74	76	0.0278	106	1
168	SNr	Midbrain	0.0232	21911	8541	84	45	0.0217	512	2
57	GRN	Medulla	0.0207	33058	4130	58	47	0.0234	295	1
164	SI	Pallidum	0.0189	107414	3793	98	51	0.0164	0	3
140	PRNr	Pons	0.0173	65264	1685	84	24	0.0189	22	1
4	ACB	Striatum	0.0168	190736	7020	67	69	0.0127	0	3
68	IRN	Medulla	0.0166	42432	2775	59	35	0.0191	111	1
47	ENTl	Hippocam Formation	0.0160	118185	34168	84	99	0.0124	431	4
55	GPe	Pallidum	0.0155	43915	6520	77	51	0.0135	53	2
129	PIR	Olfactory Areas	0.0145	112799	22312	93	45	0.0103	143	4
95	MOp	Isocortex	0.0137	105223	27542	79	119	0.0101	715	2
15	AON	Olfactory Areas	0.0130	38855	20315	81	41	0.0081	372	4
25	CA1	Hippocam Formation	0.0128	78005	2415	65	32	0.0101	105	6
94	MOB	Olfactory Areas	0.0125	45012	390	86	22	0.0081	1093	4
96	MOs	Isocortex	0.0124	119506	23453	75	133	0.0090	508	2

S2 Table. Hub Nodes. High P and Deg–in or Deg–out.

ID	Acrn	Region	P	Deg In, wt	Deg Out, wt
31	CLA	Cortical Subplate	0.7860	19,666	117,022
47	ENTl	Hippocam Formation	0.7877	118,185	34,168
32	CLI	Midbrain	0.7128	177,177	17,7177
135	PP	Thalamus	0.6987	2,775	152,884
75	LHA	Hypothalamus	0.6839	149,643	10,634
143	PT	Thalamus	0.6697	104,753	104,753
96	MOs	Isoctortex	0.6450	119,506	23,453
89	MGd	Thalamus	0.5871	3,769	112,833
4	ACB	Striatum	0.5750	190,736	7,020
117	PAG	Midbrain	0.5204	164,629	6,368
184	STN	Hypothalamus	0.4923	6,624	171,909
129	PIR	Olfactory Area	0.3823	112,799	22,312
95	MOp	Isoctortex	0.3439	105,223	27,542
161	SCm	Midbrain	0.3210	215,384	7,160

S3 Table. Comparison of Infomap modules with those found by the Louvain and the Newman spectral bisection methods. Infomap modules are list in approximately Anterior-Posterior and sensory-motor-midbrain-hindbrain order.

Infomap Module	Function / Region	Louvain Module	Newman spectral	
4	Olfactory	1	1	
2	Somaosensory / Motor	4	2	
5	Vis, Aud, TEa, RSP, PTLp	6: Aud, Tea 5: Vis, RSP, PTLp	2	
7	Association cortical areas	2, 4, 5	2	
3	Hypothalamus	1	1	
6	Hippocampus	3	1	
1	Midbrain, Pons, Medulla	1	1	
8	Cerebrum	1	1	

Figure 1. Link weights vs. distance.

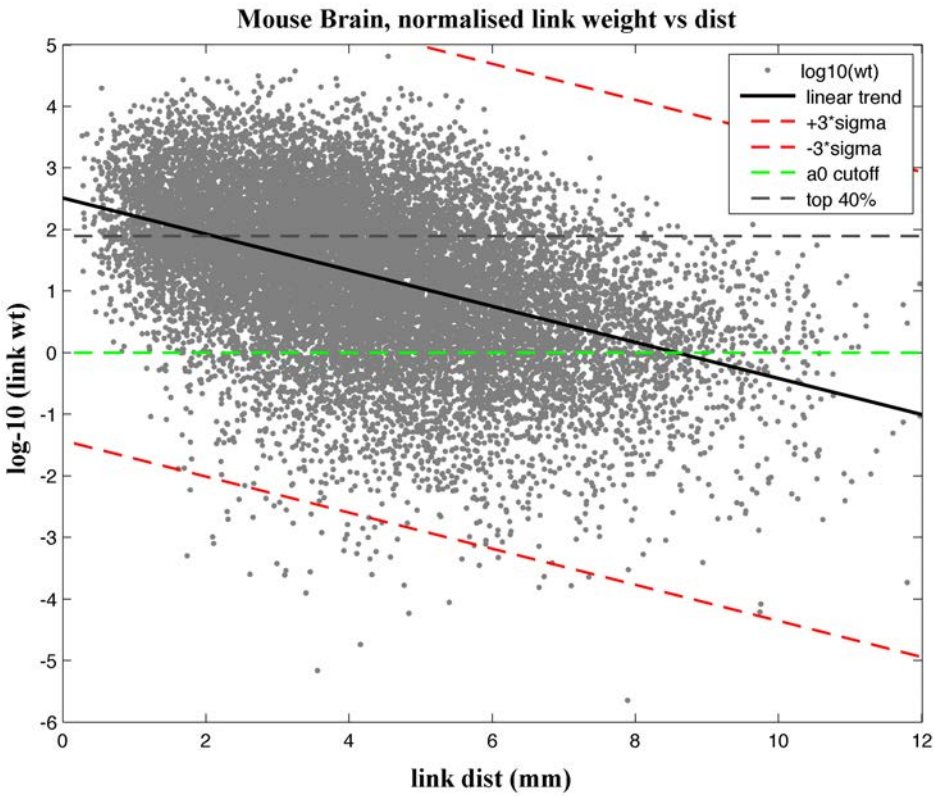

Figure 2. Network modules and brain regions.

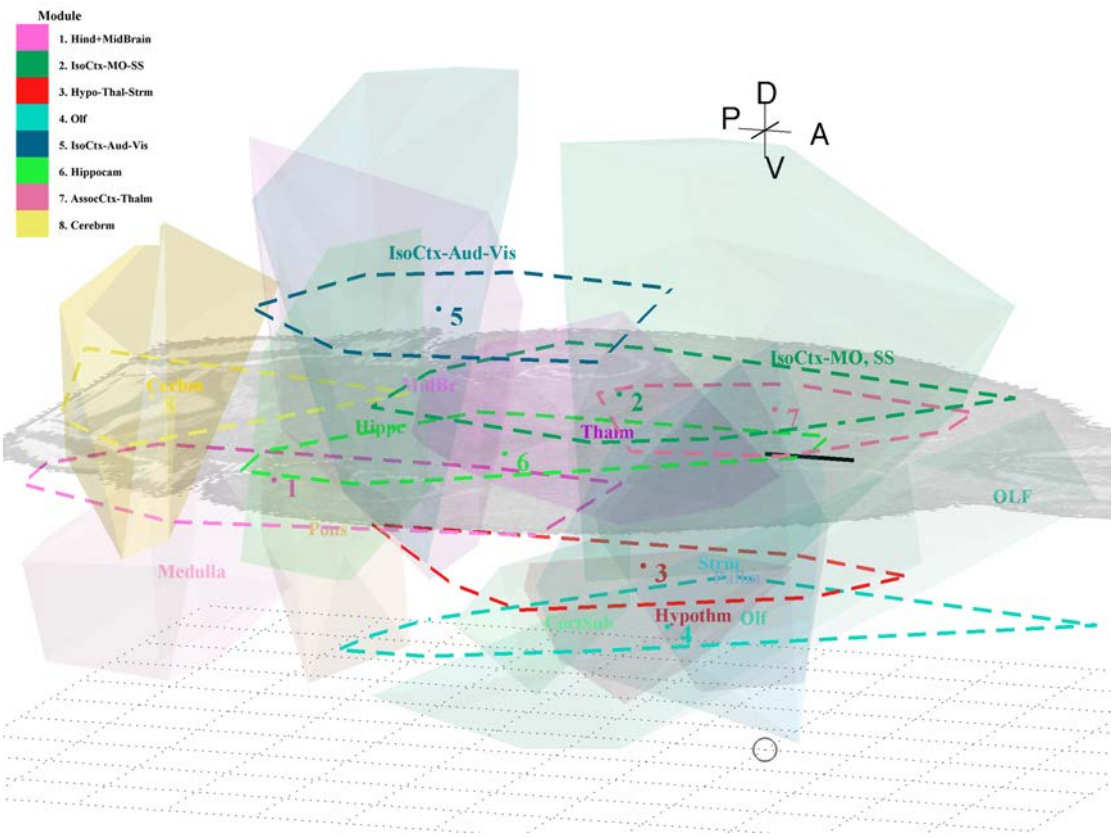

Figure 3. 3D schematic coordinates for mouse brain. a. Out links and **b**. In links.

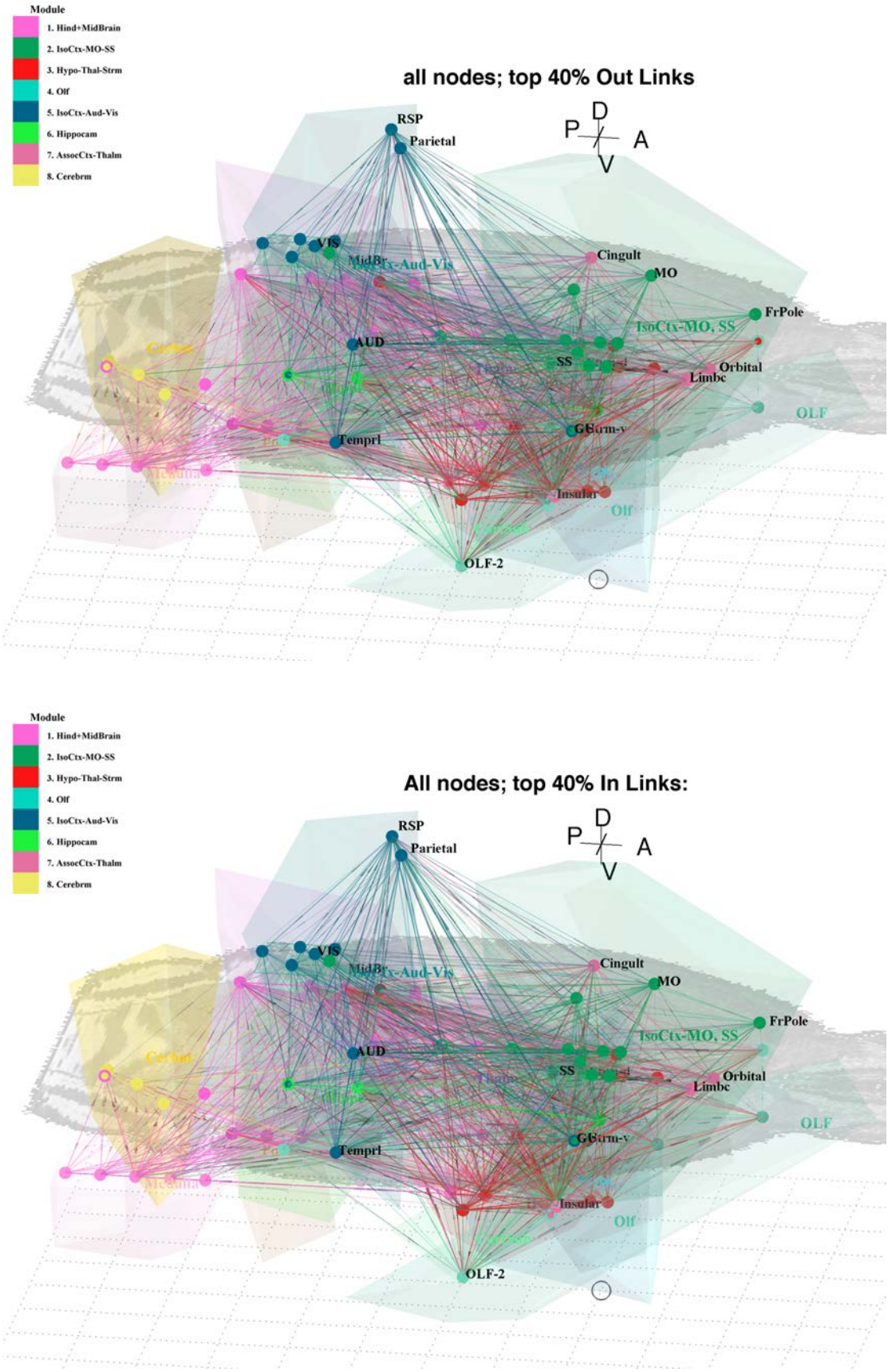

Figure 4. Primary sensory pathways. a. link distances, d < 5mm, **b**. 5 < d < 10mm.

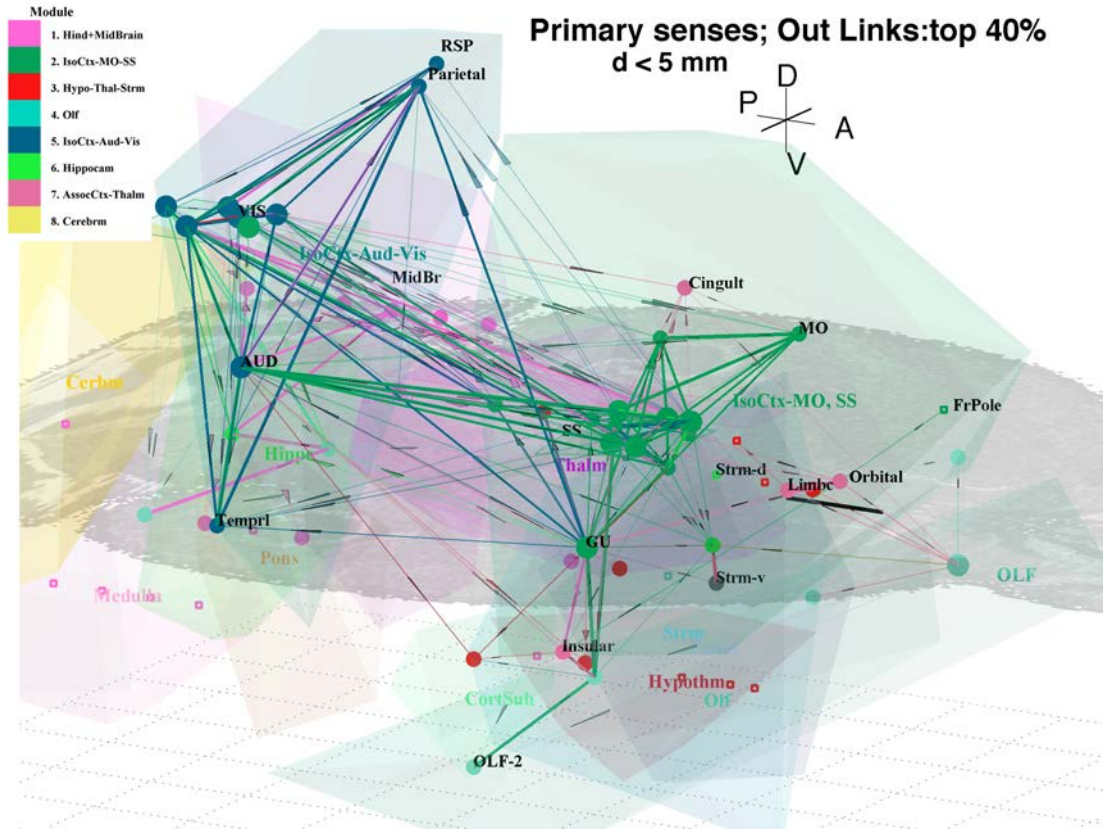

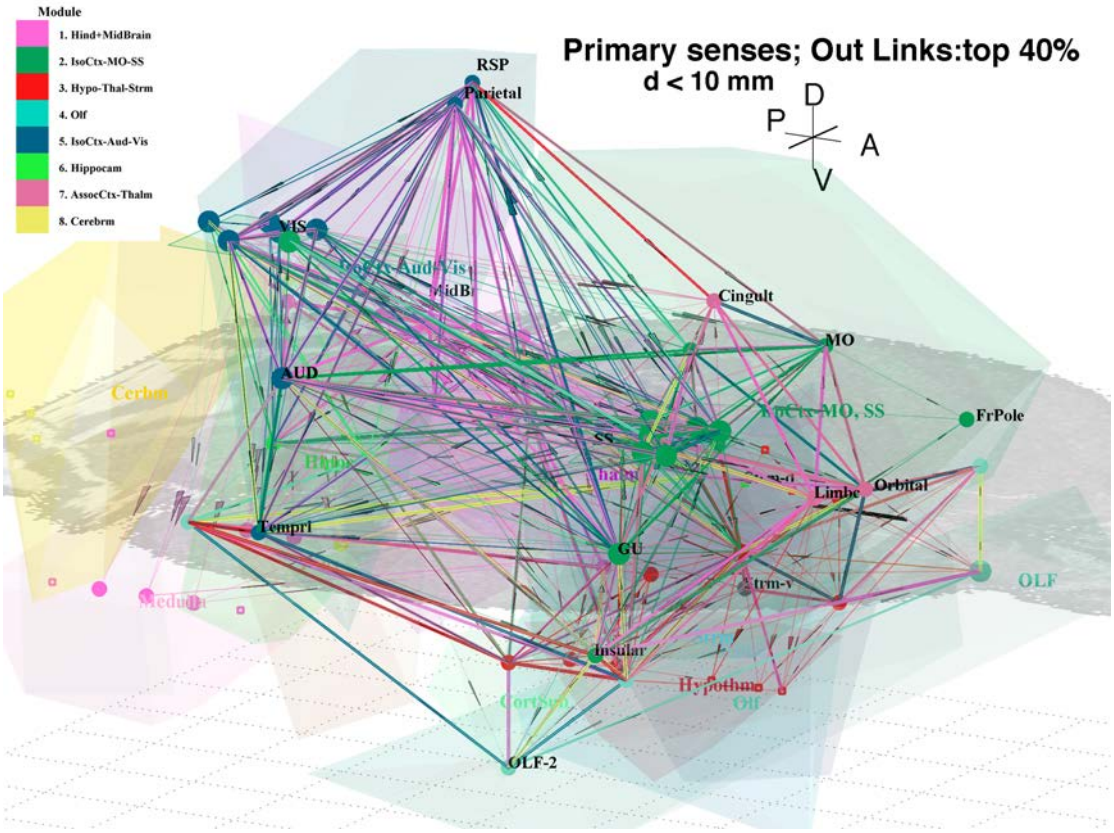

Figure 5. Anterior cortical association areas. **a**. Strong In-links, **b**. Out-links.

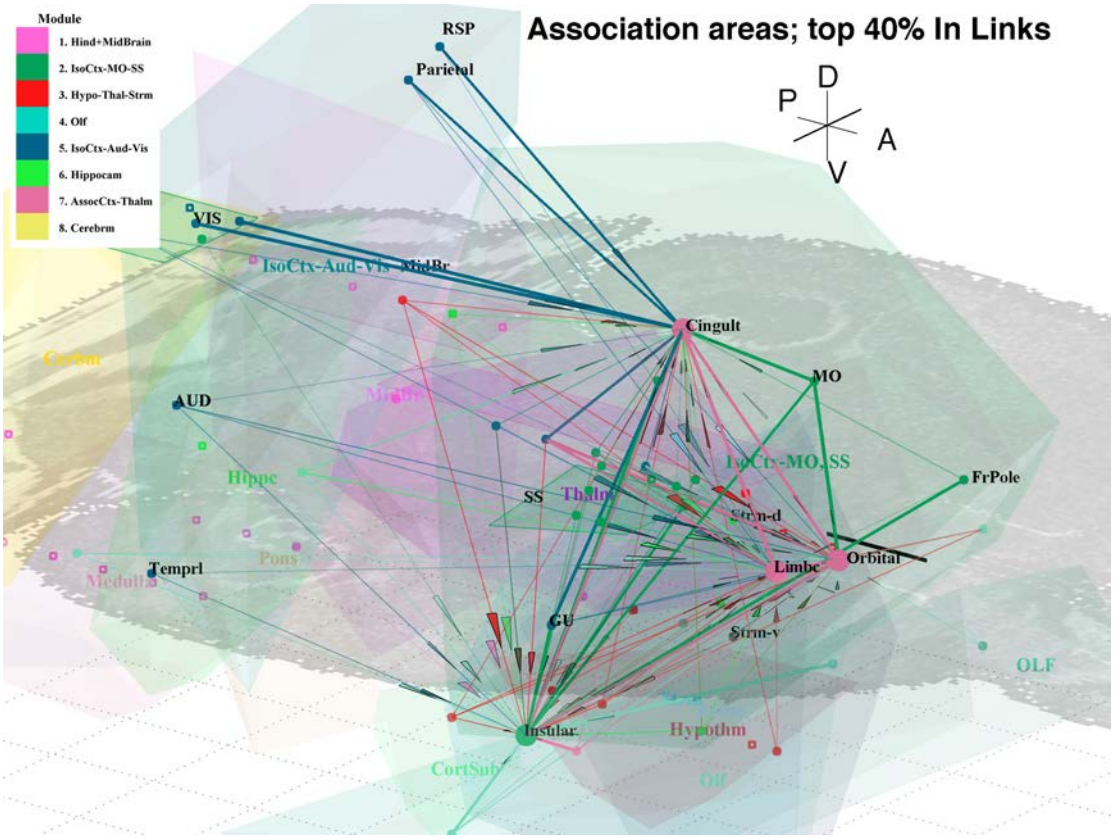

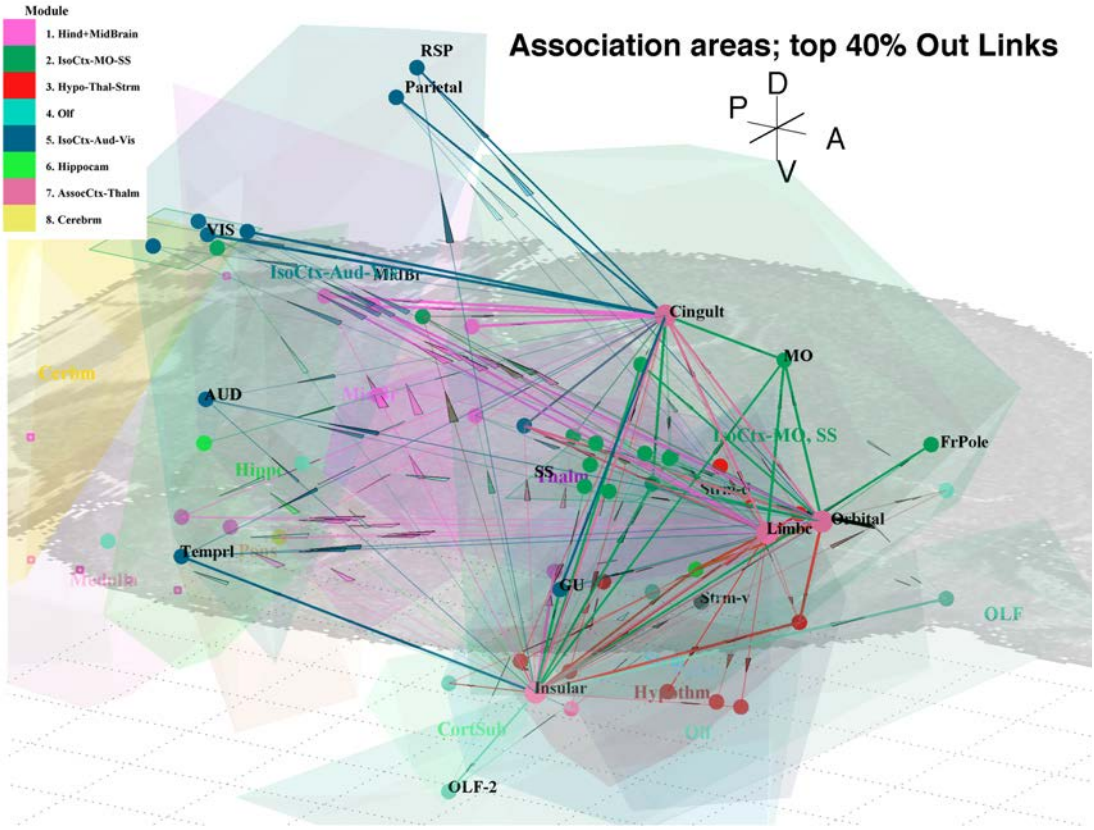

Figure 6. Posterior cortical association areas. **a**. Strong In-links, **b**. Out-links.

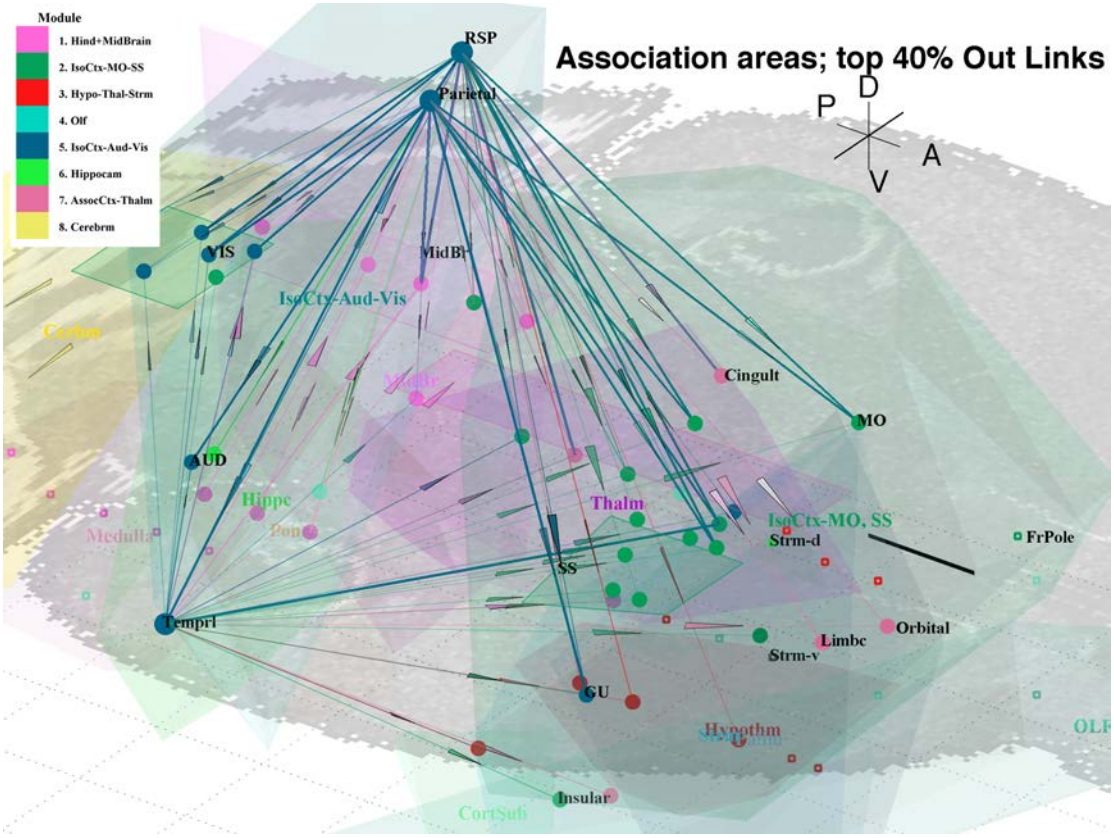

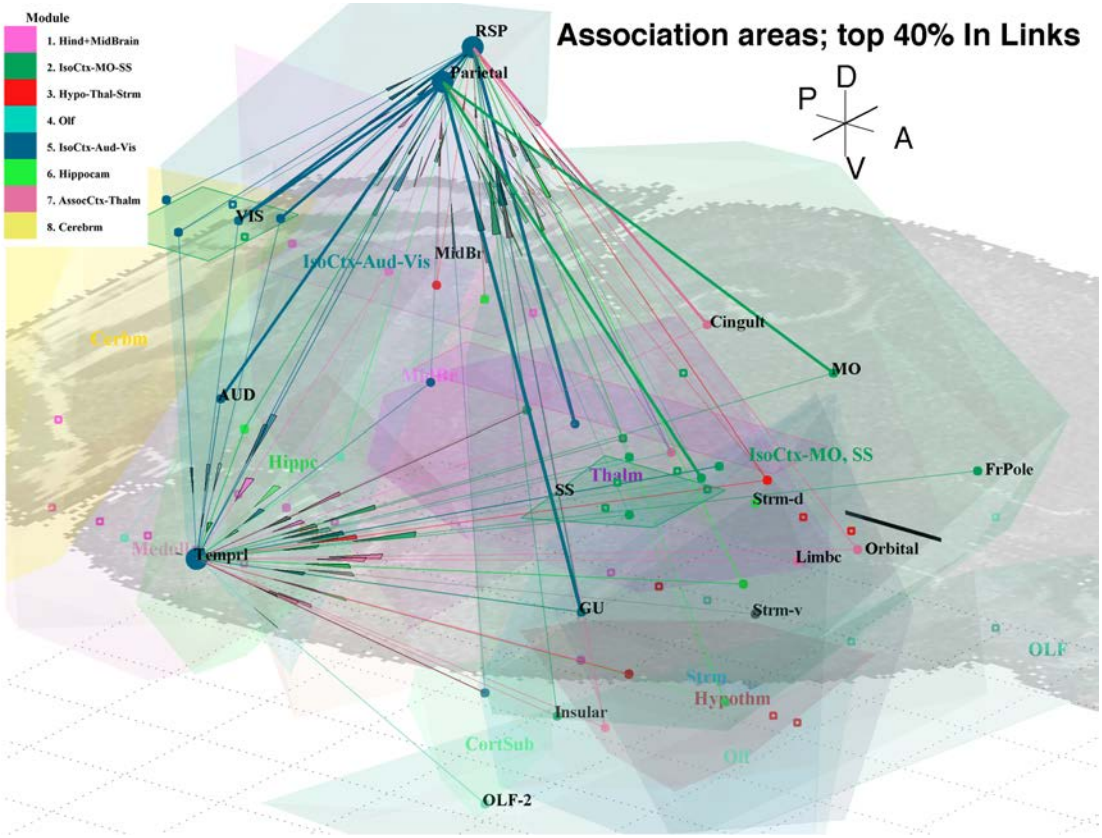

Figure 7. Cortical gradients along signal pathways.

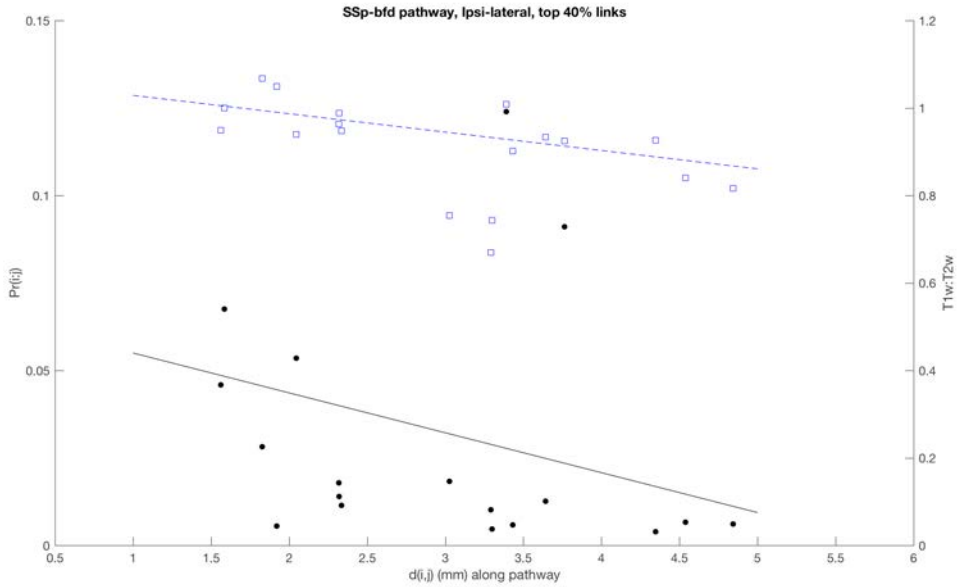

S1 Figure. All experimentally detected link strengths.

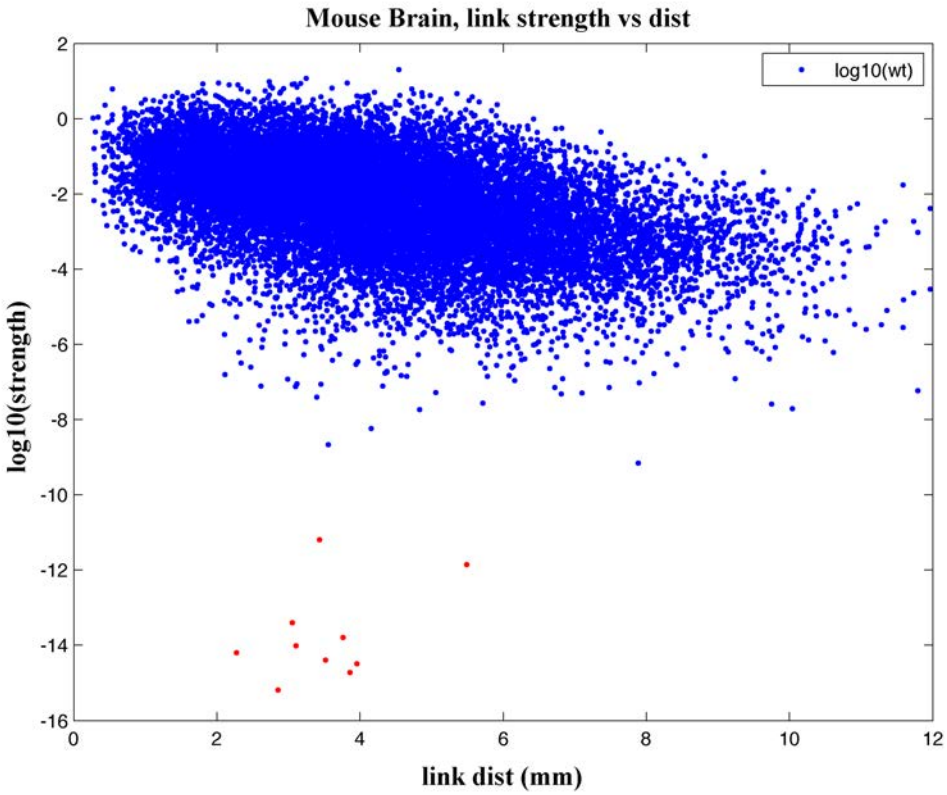

S2 Figure. **a**. Distribution of weighted Degree-In and –Out, **b**. unweighted.

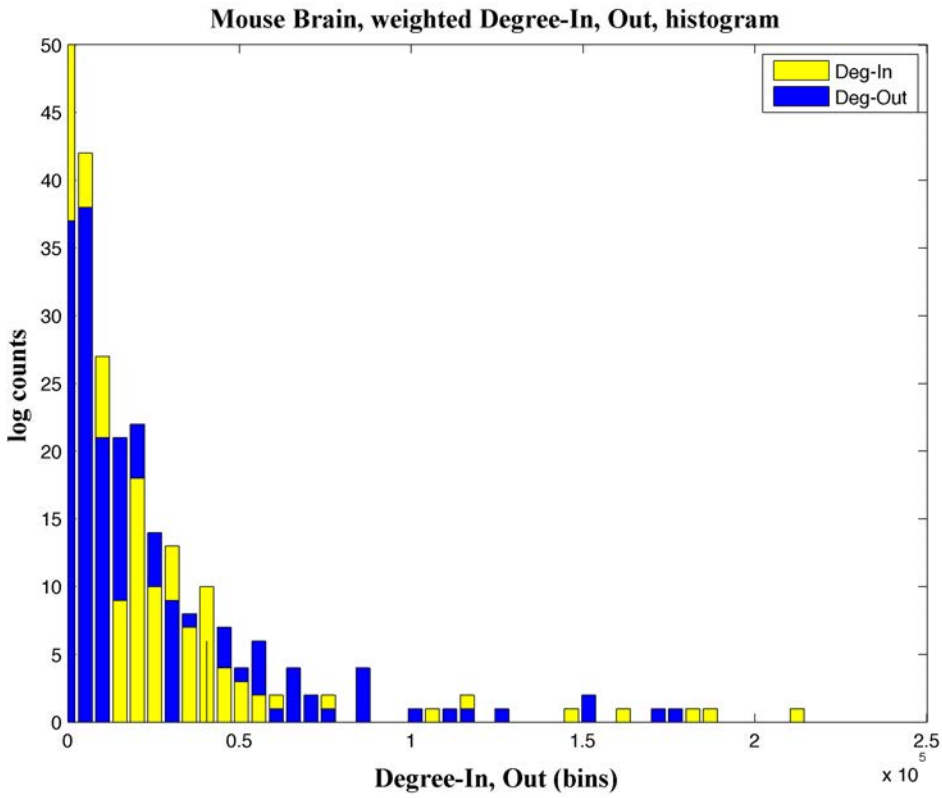

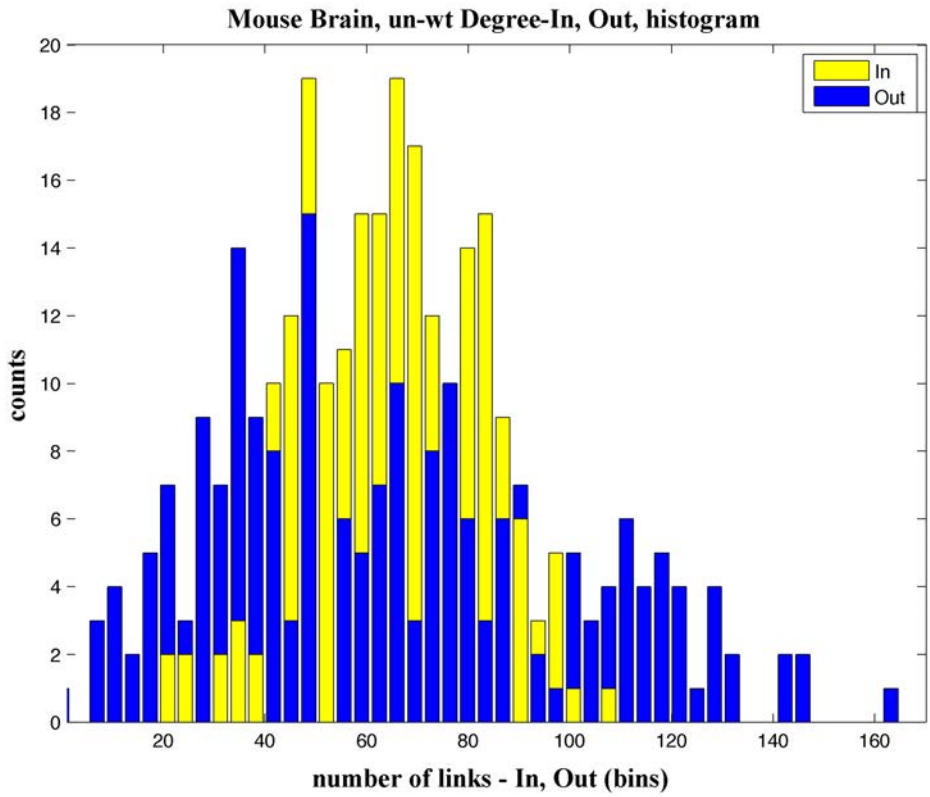

S3 Figure. a. Distribution of graph path lengths, and **b**. link distances.

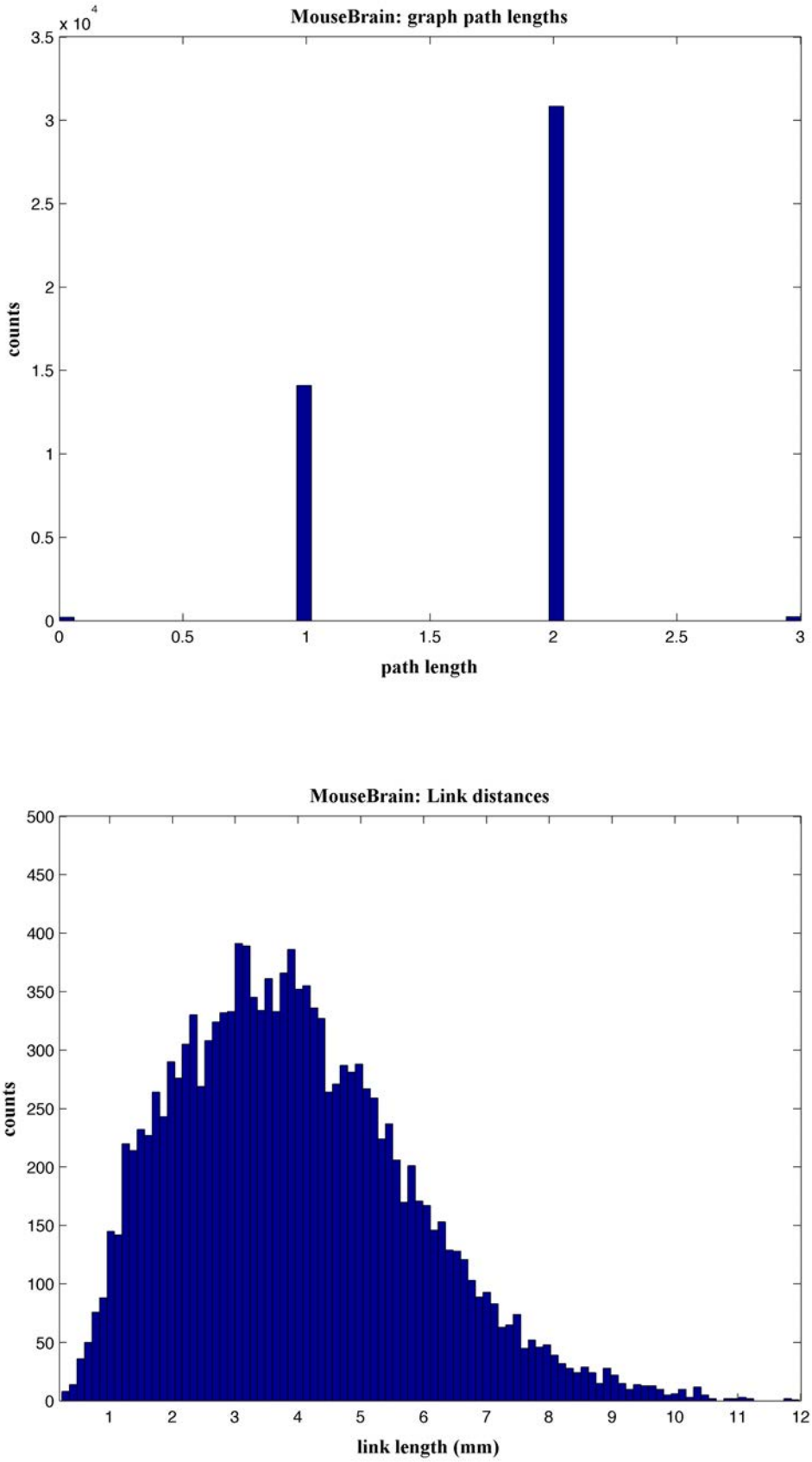

S4 Figure. All nodes plotted in Allen coordinates and their Out-links.

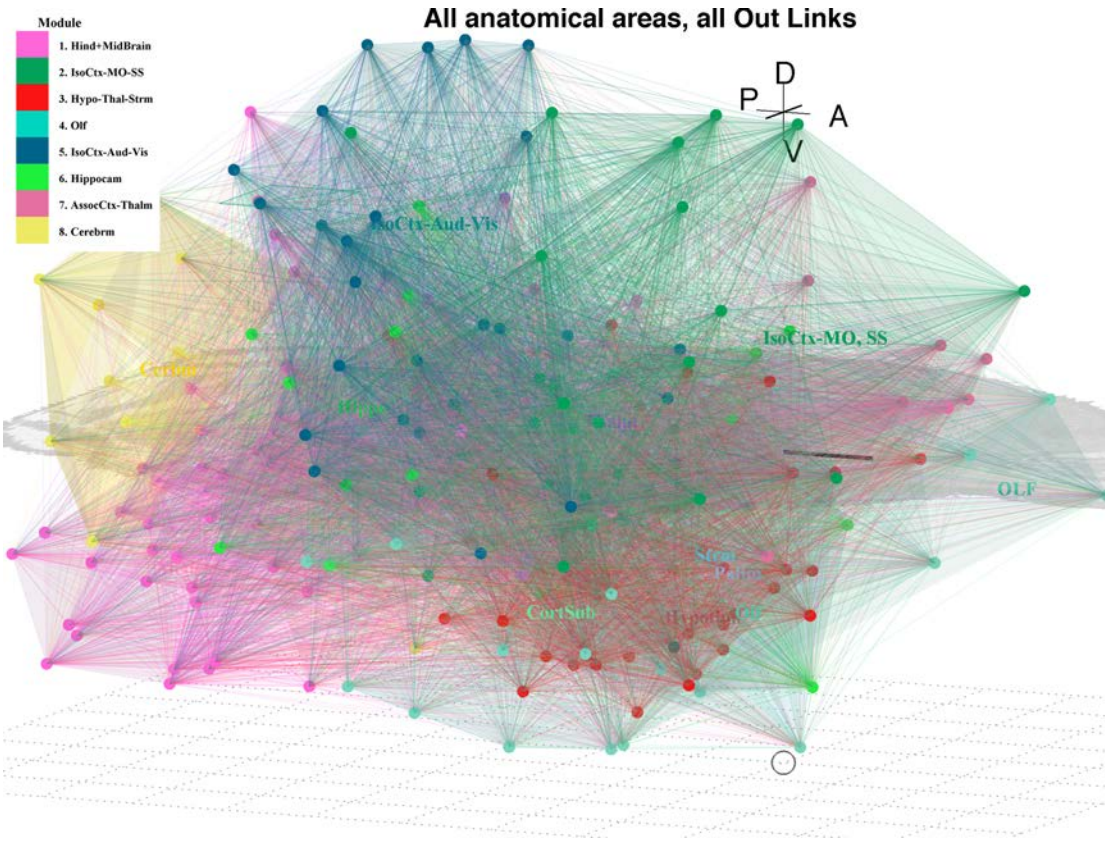

S5 Figure. **a**. Strong, medium length out links from primary sense, **b**. longer links.

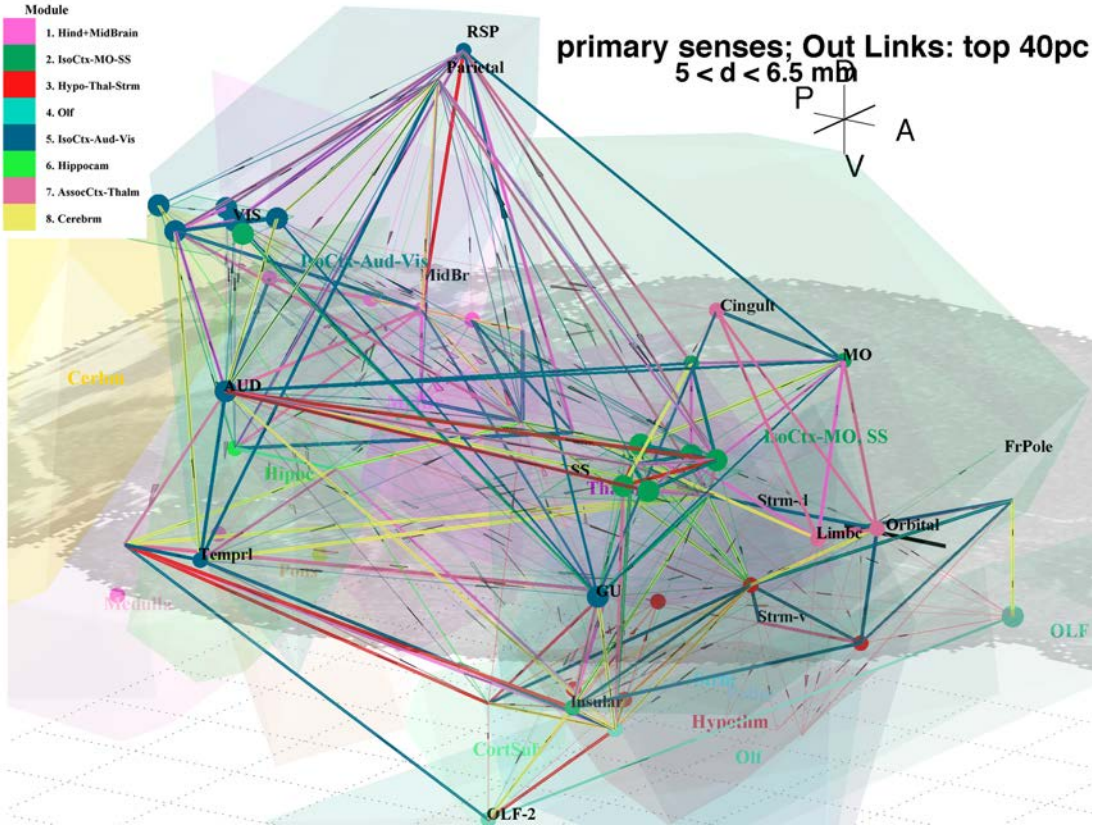

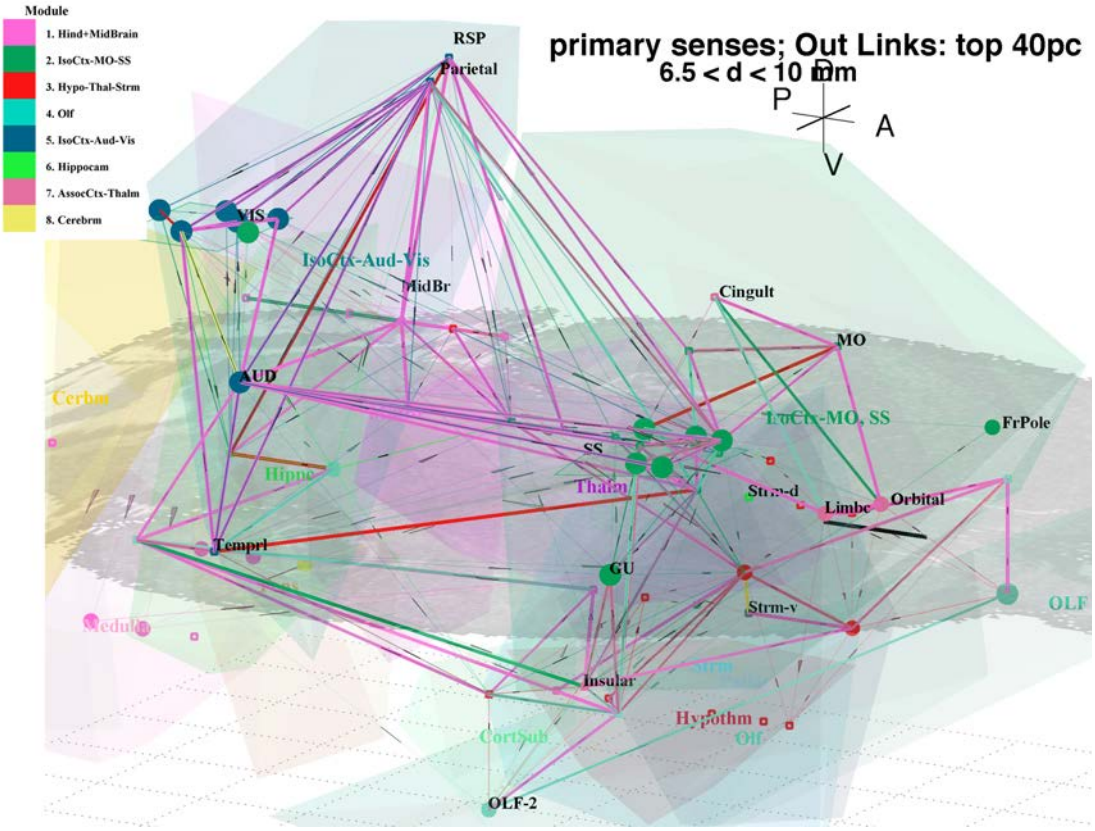

S6 Figure. Weak Out-links from primary senses, **a**. d < 6.5mm, **b**. d < 10mm.

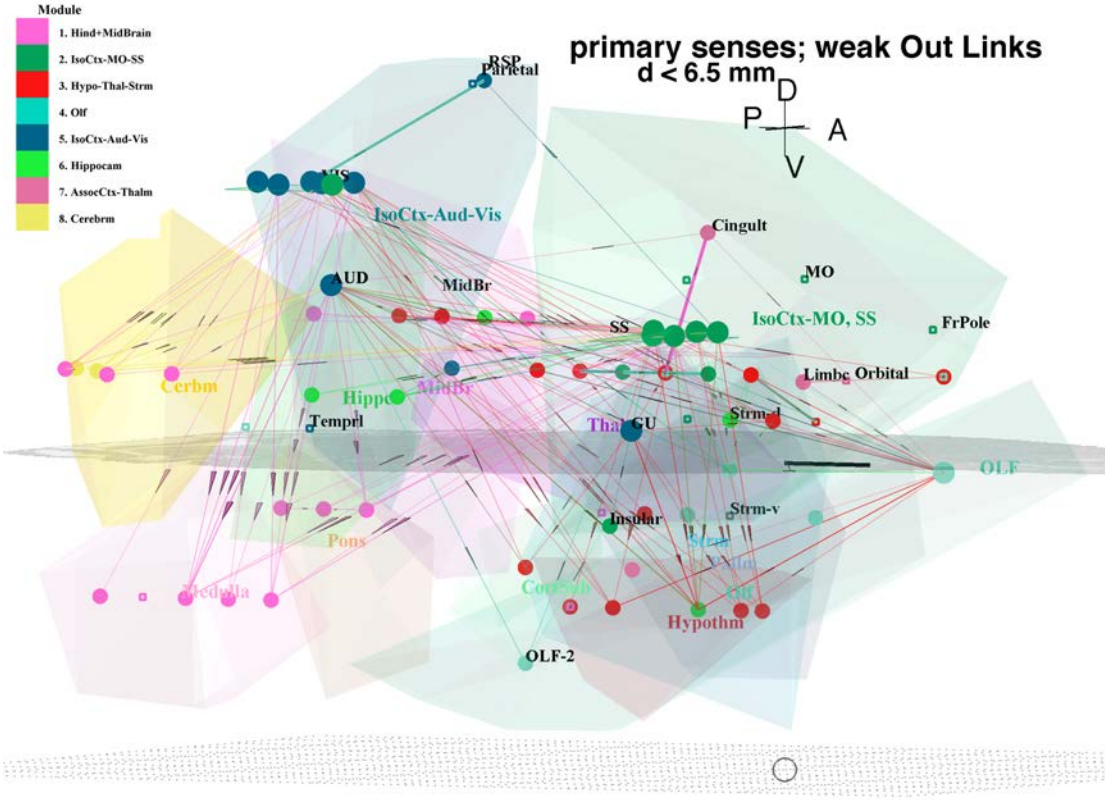

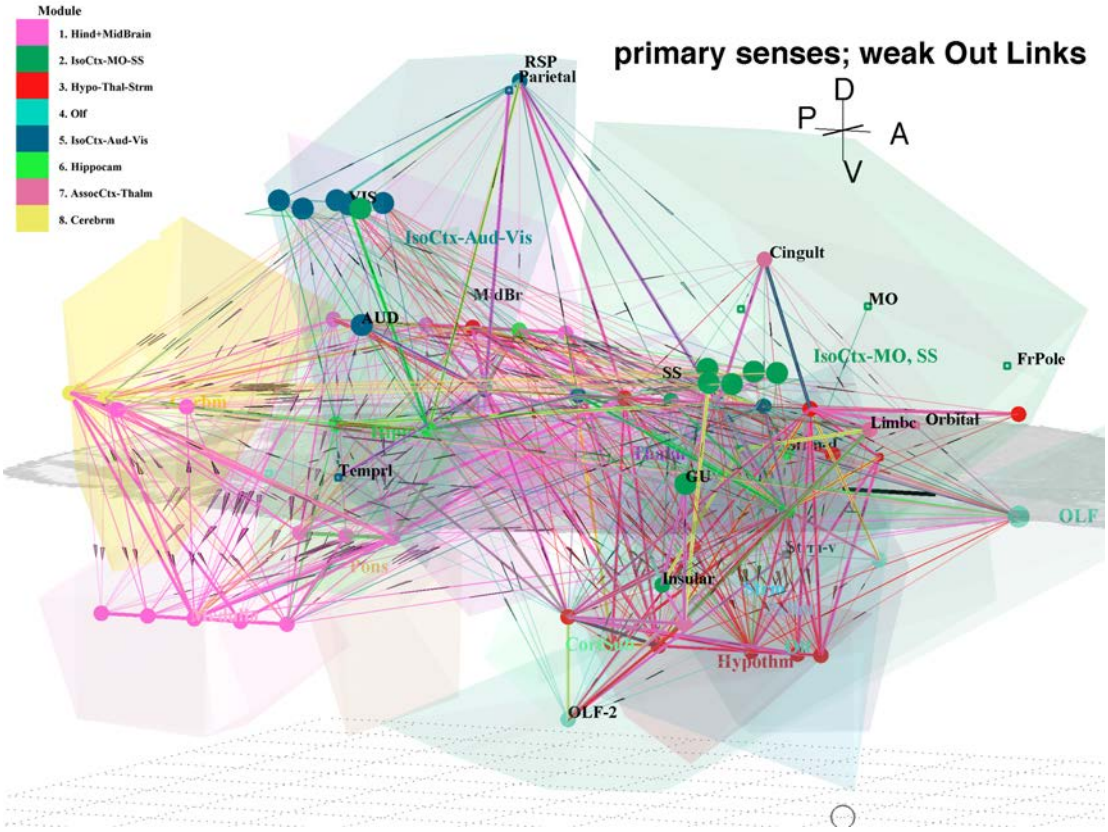

S7 Figure. **a**. Strong In- and Out-links with Frontal Pole, **b**. weak In- and Out-links.

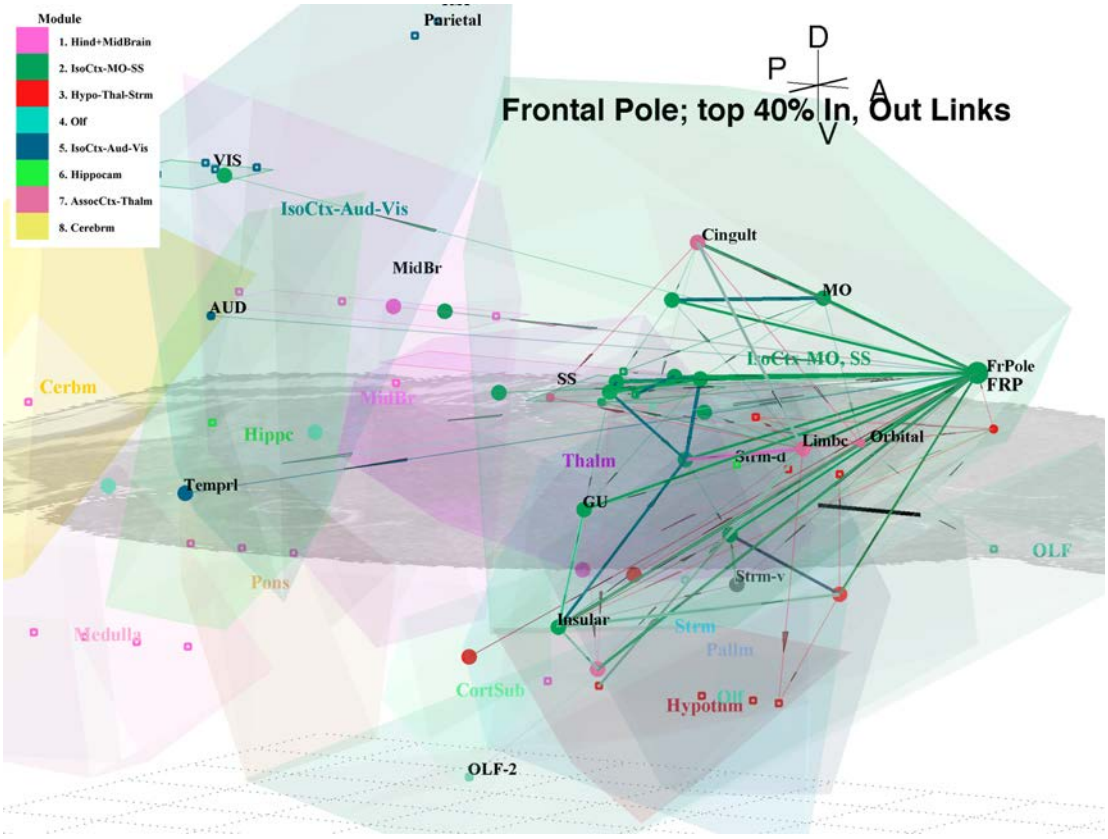

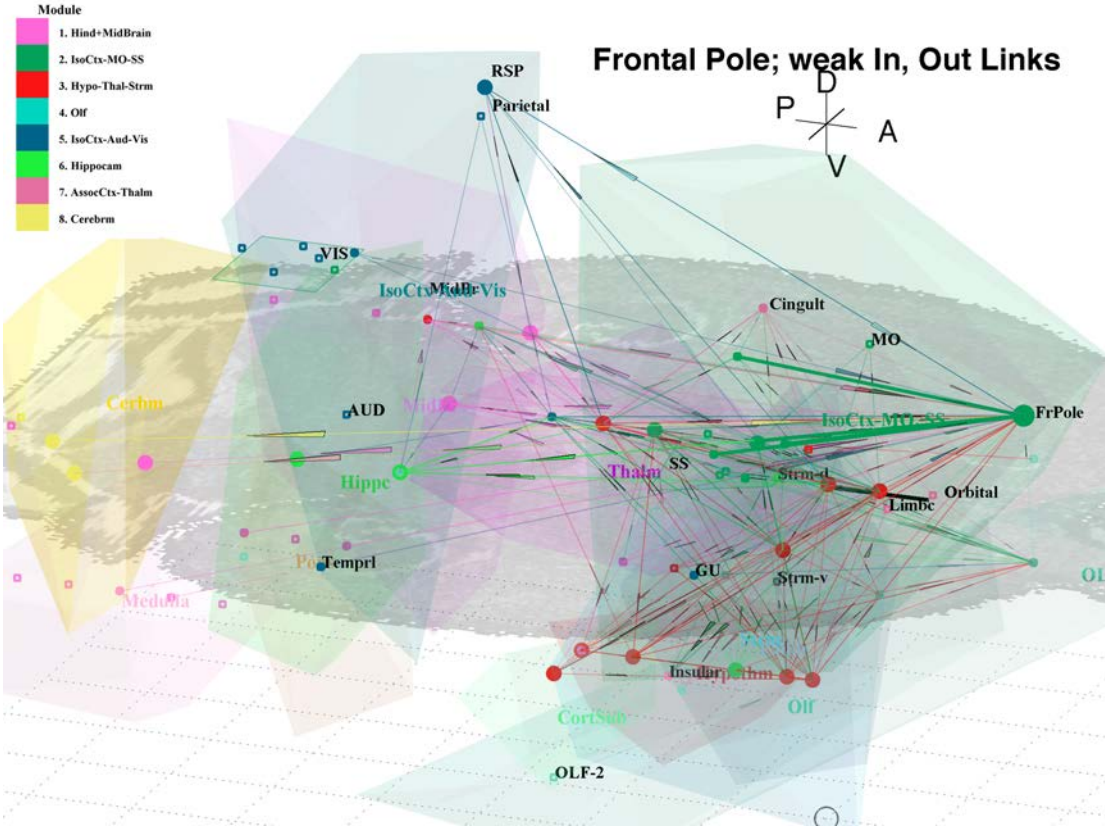

S8 Figure. Strong In-links to Motor areas (MOp, MOs).

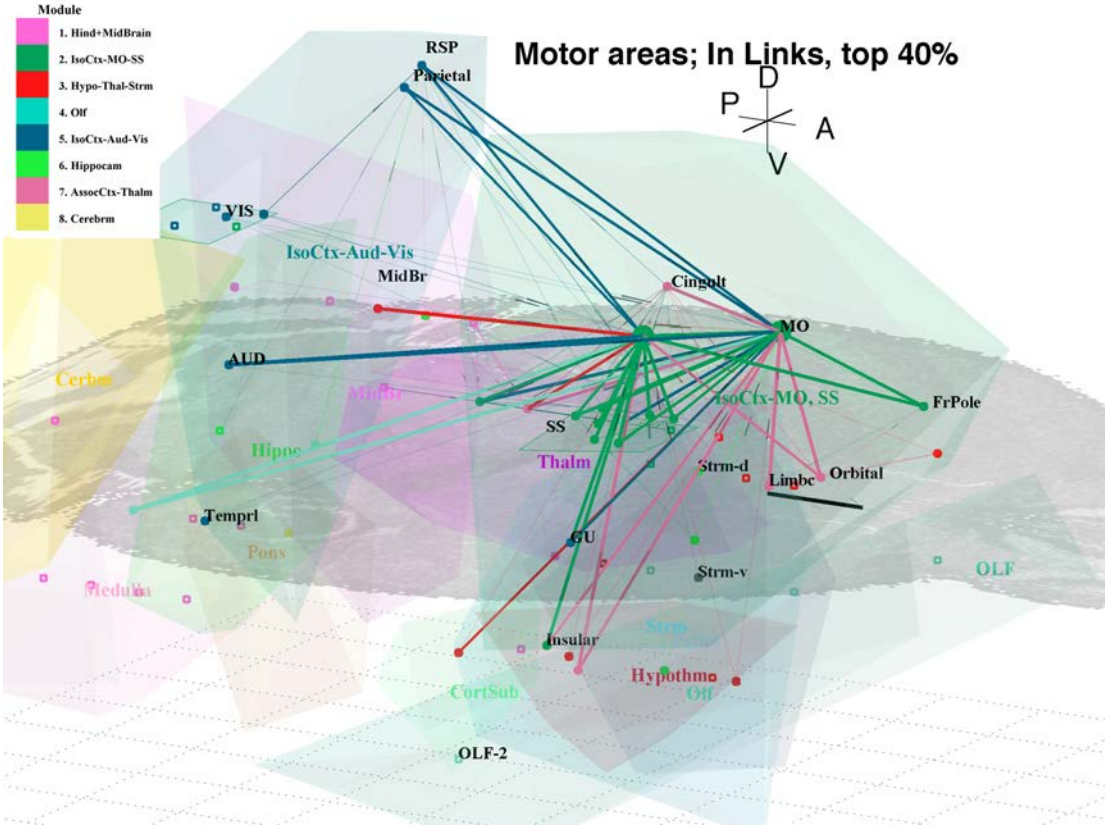

S9 Figure. Evolution of modular structure

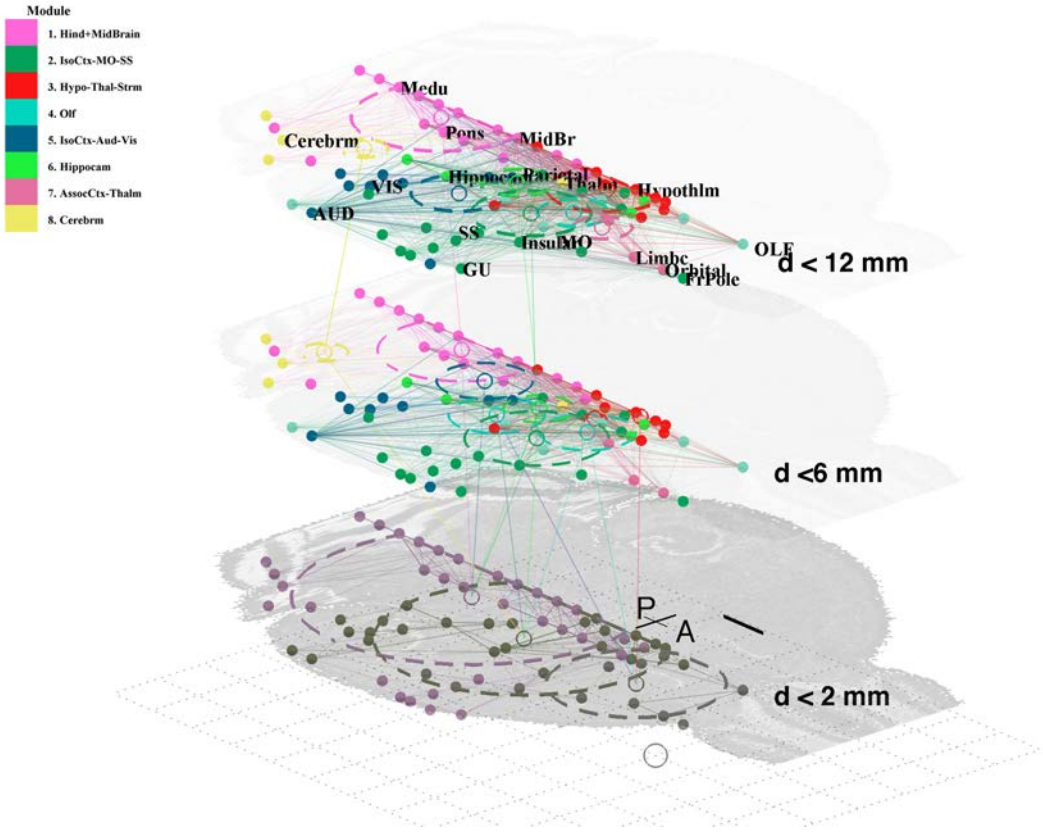
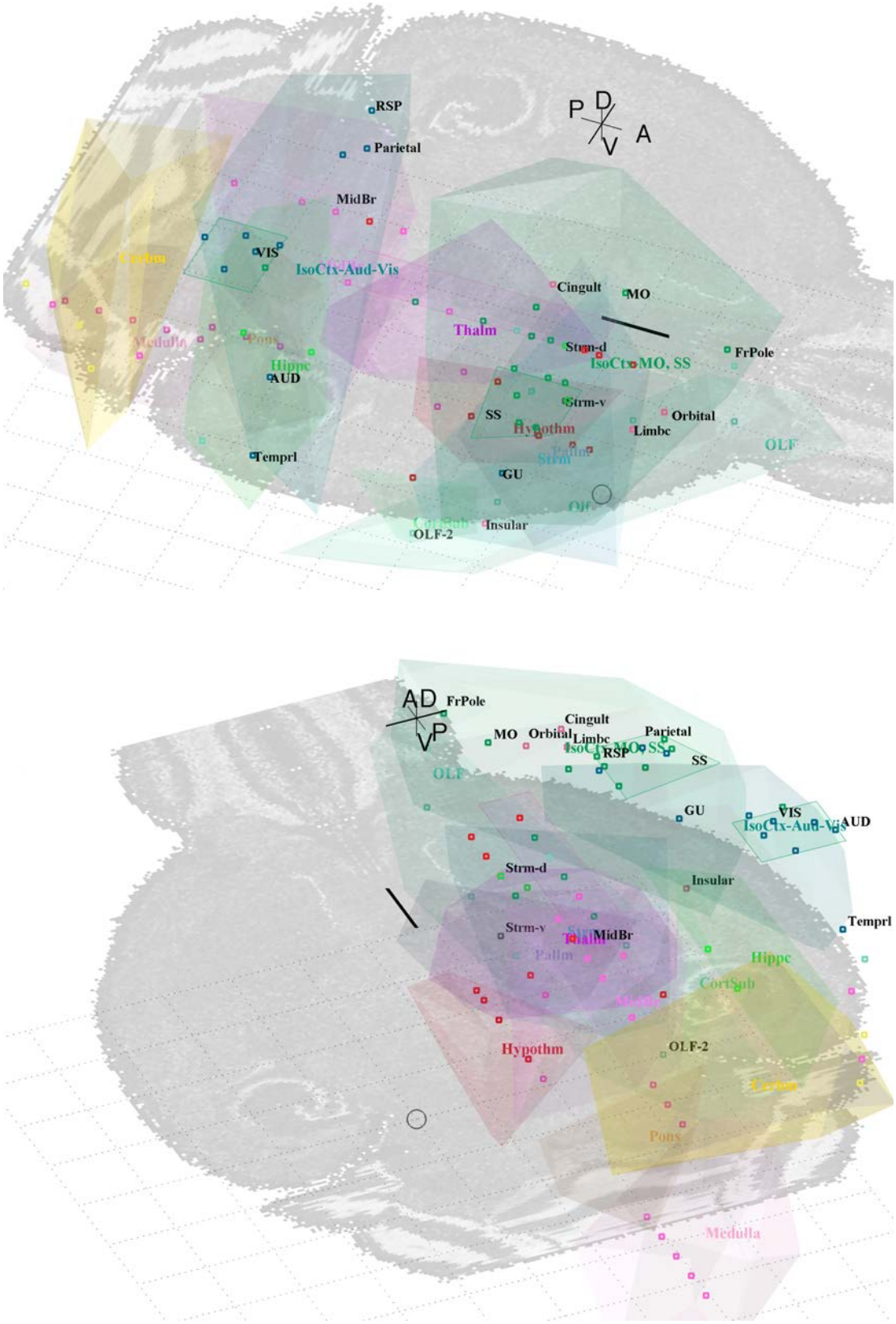
S10 Figure. All nodes in schematic coordinates. **a**. view from right front, **b**. left rear.